Chemistry and Physics Faculty Articles | Department of Chemistry and Physics

2007

Initial Mass Function Effects on the Colour Evolution of Disk Galaxies

P. Westera
University of Basel, Switzerland

M. Samland
University of Basel, Switzerland

Stefan Kautsch
University of Basel, Switzerland, skautsch@nova.edu

R. Buser
University of Basel, Switzerland

K. Ammon
University of Basel, Switzerland

Astronomy & Astrophysics

Initial mass function effects on the colour evolution of disk galaxies[*]

P. Westera, M. Samland, S. J. Kautsch, R. Buser, and K. Ammon

Astronomical Institute. Department of Physics and Astronomy, University of Basel, Venusstr. 7, 4102 Binningen, Switzerland
e-mail: [westera;buser]@astro.unibas.ch

ABSTRACT

Aims. In this work, we want to find out if the IMF can be determined from colour images, integrated colours, or mass-to-light ratios, especially at high redshift, where galaxies cannot be resolved into individual stars, which would enable us to investigate dependencies of the IMF on cosmological epoch.

Methods. We use chemo-dynamical models to investigate the influence of the Initial Mass Function (IMF) on the evolution of a Milky Way-type disk galaxy, in particular of its colours.

Results. We find that the effect of the IMF on the internal gas absorption is larger than its effect on the light from the stellar content. However, the two effects work in the opposite sense: An IMF with more high mass stars leads to brighter and bluer star-light, but also to more interstellar dust and thus to more absorption, causing a kind of "IMF degeneracy". The most likely wavelength region in which to detect IMF effects is the infrared (i.e., JHK). We also provide photometric absorption and inclination corrections in the SDSS $ugriz$ and the HST WFPC2 and NICMOS systems.

Key words. stars: luminosity function, mass function – galaxies: evolution – galaxies: ISM – dust, extinction – galaxies: photometry

1. Introduction

The determination of the Initial Mass Function (IMF) of stellar populations and the detection of its possible variations are long lasting questions in astronomy. The first IMF, a single-slope power law, was published by Salpeter (1955) based on stars in the solar neighbourhood, and is still occasionally used in stellar population studies. However, it has been known since Miller & Scalo's (1979) milestone paper on the subject that the IMF flattens at low masses. In the meantime, this finding has been confirmed in numerous works (Scalo 1986; Kroupa et al. 1993; Gould et al. 1997; Reid & Gizis 1997; Gould et al. 1998; Chabrier 2001; Piotto & Zoccali 1999; Zoccali et al. 2000, and others). Recently, Chabrier (2002) also found indications of a turn-over in the brown dwarfs regime. For recent reviews see Kroupa (2002), Chabrier (2003).

An indication of the importance of the subject is the number of IMFs produced over the years: Salpeter (1955), Miller & Scalo (1979), Lequeux (1979), Kennicutt (1983), Scalo (1986), Ferraro et al. (1997), Piotto et al. (1997), Scalo (1998), Carigi et al. (1999), Kroupa (2001) (universal and present day IMFs), Chabrier (2001), and others.

Another important issue are variations of the IMF with the star forming conditions (pressure, density, metallicity of the forming cloud, etc.). Although such variations are predicted, only little evidence of them has been found so far (Kroupa 2001). We expect especially at high redshift to see differences from the present-day IMF, as the lower metallicity of the star-forming clouds is expected to cause higher temperatures and thereby higher average stellar masses (Larson 1998). Unfortunately, high redshift galaxies are too faint to be resolved into individual stars,

which makes it difficult, if not impossible, to determine their IMFs. Therefore, it would be interesting to know if other, more global observables, such as integrated spectra or colours, can also yield some information about the stellar IMF. The IMF influences the light of a galaxy not only directly through the contributions of the stars of different (birth) masses, but also indirectly by affecting the entire evolution. The fraction of high mass stars determines the gas- and "dust"-yield of the partial populations and, hence, the star formation history (SFH) from the second stellar generation on, as well as the gas absorption. For these reasons, we hope to be able to see signatures of the IMF even in the integrated light of galaxies.

For this purpose, Portinari et al. (2004) studied the influence of the IMF on the (I band) mass-to-light (M/L) ratio of galactic disks (Sbc/Sc) using chemo-photometric models and adopting 6 different IMFs, including the Salpeter (1955) and Kroupa (1998) IMFs, which is interesting in connection with this work, because in the present work, we also compare models using the Salpeter IMF and a more recent IMF by Kroupa. For each IMF, they calculate chemical evolution models with infall, metallicity gradients, and SFHs representative of late-type spiral disks (but not varying with the IMF). They find that so-called "bottom-light" IMFs (i.e., with less low-mass stars than Salpeter) yield low M/L ratios ($\sim 0.7-1$), in agreement with various dynamical arguments and cosmological simulations. However, they calculate only stellar M/L ratios without taking into account gas absorption.

In this work, we use fully consistent 3-dimensional chemo-dynamical models by M. Samland to calculate the evolution of two galaxies, with the same boundary conditions (cosmology, gas infall history, etc.), but adopting different IMFs: the Salpeter and the Kroupa (2001) "universal" IMFs. Although these are not the most state-of-the-art IMFs available, they were chosen

---

[*] Appendices A–D are only available in electronic form at http://www.aanda.org

because of their clear differences in their low-to-high-mass stars ratios, so any IMF-induced differences should appear clearly. The spectra and (Hubble Space Telescope (HST), SLOAN Digital Sky Survey (SDSS) and Washington) colour images and integrated colours were then calculated using the same method as in Westera et al. (2002b). An important advantage of our programme is that we can disentangle different effects on the spectral properties of a model galaxy, such as of internal absorption, by artificially blinding these contributions out, and then recalculating the spectral properties.

The outline of this paper is as follows: Sect. 2 describes the physics and properties of the two chemo-dynamical models, and in Sect. 3, it is explained how the spectral properties of these models were calculated. Section 5 contains the results, and a comparison of the model colours with SDSS data, which were extracted in the way described in Sect. 4. In Sect. 6, we draw some conclusions and give a brief summary.

2. The chemo-dynamical models

The models simulate the formation of a $8 \times 10^{11}\ M_\odot$ galaxy leaving all parameters, except for the IMF, the same for both models. The models are for a Milky Way-type galaxy, but we expect our results (IMF effects) to be similar for other disk galaxies, as the properties, which are important for the colour evolution (star formation history, gas feedback and enrichment, etc.) probably depend in a similar way on the IMF for different types of disk galaxies.

The two models have different IMFs implemented, a Salpeter (1955) IMF, which is a one-segment potential law with an exponent $\alpha = 2.35$ in the mass range from 0.1 to 50 $M_\odot$, and a Kroupa "universal" (also called "standard" or "canonical") IMF (Eq. (2) of Kroupa 2001), a two-segment law with $\alpha = 1.3$ from 0.08 to 0.5 $M_\odot$ and $\alpha = 2.3$ from 0.5 to 50 $M_\odot$, respectively, in order to investigate the influence of the IMF shape on the formation processes of a disk galaxy. The main difference between the two IMFs lies in the high-to-low mass stars ratio, in the sense that a population with a Kroupa IMF has more high-mass stars than a population of the same mass, but with a Salpeter IMF.

The 3-dimensional chemo-dynamical models are of the same type as those described in Samland & Gerhard (2003); so here, we only summarise very briefly the main properties, but take a more detailed look at the few quantities that will become interesting for the interpretation in Sect. 5: the (stellar) mass surface density, the stellar particle ages, the stellar metallicities, and the gas density and metallicity.

The models take into account initial cosmological and environmental conditions, but also internal feedback processes, such as heating by supernovae, dissipation, radiative cooling, nucleosynthesis, and in- and outflows. Since they are fully self-consistent models, they include dark matter, stars and the different phases of the interstellar medium (ISM), as well as the processes ("chemistry") which connect the ISM and the stars.

More quantitatively, the models assume a flat Universe with the following cosmological parameters: $H_0 = 70\ \mathrm{km\ s^{-1}\ Mpc^{-1}}$, $\Omega_0 = 0.3$, $\Omega_\Lambda = 0.7$, and $\frac{M_{\mathrm{Bary}}}{M_{\mathrm{Dark}}} = \frac{1}{8}$. The total spin parameter of the model galaxies was chosen to be $\lambda = 0.05$ (Barnes & Efstathiou 1987), and the angular momentum distribution was calculated according to Bullock et al. (2001) using $\mu = 10$. We follow the evolution from $z = 9.5$ (corresponding in this cosmology to an age of the Universe of 0.5 Gyr) until $z = 0$ (13.5 Gyr).

The models are characterised by a slowly growing dark halo and a continuous gas infall following the universal mass
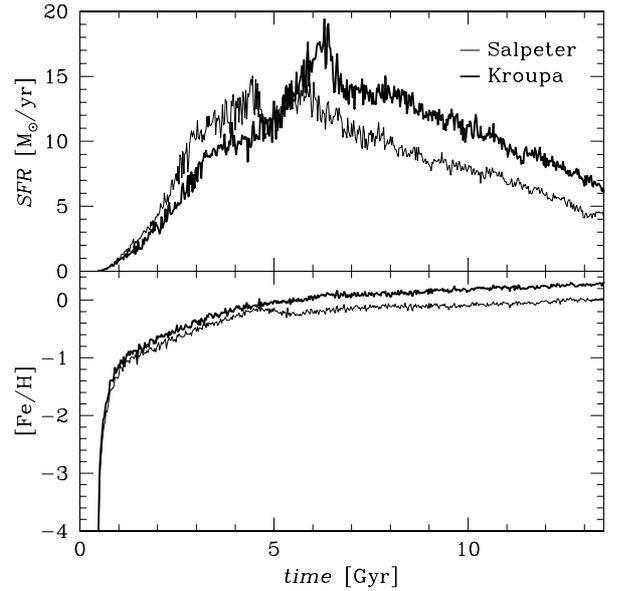

Fig. 1. Star formation histories of the Salpeter (thin) and Kroupa (thick) models. *Top panel*: star formation rates, *bottom panel*: average star formation metallicities.

accretion histories found by van den Bosch (2002) and Wechsler et al. (2002) using a formation redshift $z_{\mathrm{Formation}}$ of 4.0 and a total mass M of $8 \times 10^{11}\ M_\odot$. As the gas infall continues until the present day, we expect for both models a mixture of stellar populations of many different ages.

However, the two models do not show the same SFH. As the Kroupa IMF features more high mass stars, star formation will result in a stronger heating by stellar radiation, more stellar wind, more feedback from supernovae I and II and thus a higher mass return and metal yield. As a result, the Kroupa model has a lower SFR than the Salpeter model for the first ~5 Gyr, due to the heating from the stellar winds from the first generations. Afterwards, that is after ~5.5 Gyr, the Kroupa model has a higher SFR due to the larger available amount of gas (as seen in Fig. 2, top panel). After around 7.5 Gyr, this higher SFR has compensated for the lower SFR in the beginning, so from that point on the total stellar mass is higher in the Kroupa model galaxy. In the end (at 13.5 Gyr or redshift 0), the total stellar mass amounts to $1.07 \times 10^{11}\ M_\odot$ in the Salpeter model and to $1.25 \times 10^{11}\ M_\odot$ in the Kroupa model. The two SFRs can be studied in detail in Fig. 1 (top panel), from which can also be seen that the SFR remains significant until the present epoch, as expected from the gas infall history. The bottom panel shows the average star formation metallicity.

The average gas metallicities [O/H] of the models (shown in Fig. 2, middle panel) increase most steeply during the phases of maximum star formation. They start at [O/H] $\simeq -4$, and reach their present values of ~−0.1 dex or ~+0.2 dex at $z \simeq 1$. This higher gas metallicity of the Kroupa model, combined with the higher gas density (top panel of Fig. 2), causes the Kroupa model galaxy to contain about twice as much metals in the interstellar matter (ISM), or "dust", as the Salpeter galaxy, which can be seen in the bottom panel of Fig. 2.

The output quantities of interest (which are the input quantities for the programme which calculates the spectral properties) are the following, at each time step: a number of stellar particles, each with its spatial position, initial mass, age, and metallicity, as well as the gas density and metallicity on a 3-dimensional grid
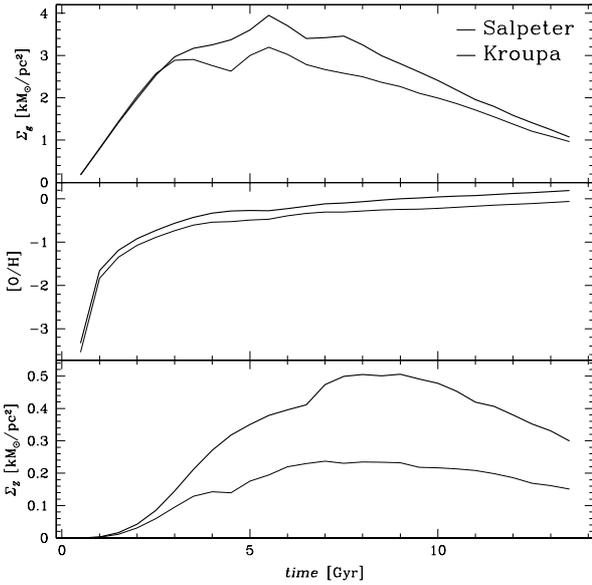
Fig. 2. Average gas column densities (*top panel*), gas metallicities (*middle panel*), and "dust" gas column densities, that is $Z_g * \Sigma_g$, of the Salpeter (thin) and Kroupa (thick) models.

covering the galaxy out to where the gas density is negligible (100 kpc), as a function of time.

Figure 3 shows the stellar mass distributions of the two models projected face-on and edge-on. Both models result in disk galaxies with weak spiral arms, whereas the Salpeter model produces a bulge 2 Gyr sooner (at ~4 Gyr) than the Kroupa model, which can be seen in the second row of Fig. 3 ($z = 1.2156$, which corresponds to 5 Gyr). In the Kroupa model (right two panels), the bulge is not yet present at this epoch, but in the Salpeter model (left two panels), it is. This can also be seen in the profiles (Fig. 4, second row). This delay in bulge formation in the Kroupa model is probably also due to stellar winds. As soon as the bulge appears in either model, we also see a plateau in the mass profiles at around 2 to 5 kpc. This is due to stellar winds from the bulge, which push out the gas from the inner disk (at 2 kpc) to a distance of 4 kpc, where Star Formation then takes place. It is not bar-induced as in the more massive galaxy studied by Samland & Gerhard (2003). The fact, that, in Fig. 3, the Kroupa model galaxy seems to have a thicker disk than the Salpeter one, is just a by-eye impression. We calculated the thick and thin disk scaleheights for both models as functions of time, but found no significant differences between the models.

3. From theoretical quantities to colours and spectra

To derive 2-dimensional colour images (HST (WFPC2 and NICMOS), SDSS *ugriz*, Washington $CNT1T2$, and other photometric systems) from the star and gas distributions of the galaxy models, we proceeded in the following way:

First, two libraries of simple stellar population (SSP) spectra were produced: one with a Salpeter IMF from 0.1 to 50 $M_\odot$, and one with a Kroupa IMF from 0.08 to 50 $M_\odot$, in accordance with the galaxy models. With the Bruzual & Charlot (2000) Galaxy Isochrone Spectral Synthesis Evolution Library (GISSEL) code (Charlot & Bruzual 1991; Bruzual & Charlot 1993, 2003), integrated spectra (ISEDs) of populations were calculated for a grid of population parameters consisting of

7 metallicities ([Fe/H] = −2.252, −1.65, −0.65, −0.35, 0.09, 0.447, and 0.748) and 221 SSP ages ranging from 0 to 20 Gyr. As input, we used Padova 1994 isochrones (Fagotto et al. 1994; Girardi et al. 1996). There exist more recent versions of the Padova isochrones, Padova 2000 (Girardi et al. 2000), but there is some doubt as to whether these newer tracks produce better agreement with observed galaxy colours than the Padova 1994 models (Bruzual & Charlot 2003). Furthermore, the Padova 1994 isochrones cover a wider range of metallicities. The spectral library used was the BaSeL 3.1 "WLBC 99" (Westera 2001; Westera et al. 2002a) stellar library. The spectra of this ISED library contain fluxes at 1221 wavelengths from 9.1 nm to 160 μm, comfortably covering the entire range where galaxy radiation from stars is significant. The GISSEL software also has a higher resolution stellar library implemented, STELIB, which has a resolution high enough to study spectral (absorption) lines (1 Å in the relevant wavelength range), but, with 6900 flux points per spectrum, these spectra proved too large in terms of memory and CPU time to be included in our programme.

After choosing (through three angles) the viewing direction with respect to the galaxy principal plane, and the size (up to 320 × 320 pixels) and resolution for the "virtual CCD camera", the stellar particles are grouped into pixels. For each stellar particle, the spectrum is (geometrically, flux point by flux point) interpolated from the ISED library. For metallicities lower than the range covered by the library, the spectra for the lowest metallicity ([Fe/H] = −2.252) were used. This should not pose any problems, as trends of spectral properties with metallicity are expected to become weak below [Fe/H] = −2.0, and these lowest-metallicity stellar particles become negligible in number very soon. For SSPs of 50 Myr and younger, we added nebular emission to the spectra in the same way as described in Leitherer et al. (1999), and accordingly removed the flux below 912 Å. On the other hand, the emission of HII regions is not implemented. The inclusion of HII regions, as well as planetary nebulae and supernovae, will be one of the next steps in improving the programme.

Then, the spectra were reddened as follows, using the gas density and metallicity in the model to trace the three-dimensional distribution of dust: For each stellar particle, the metallicity-weighted gas density was integrated along the line of sight to derive the absorption coefficient A_V according to Quillen & Yukita (2001):

$$A_V = \frac{1}{50 \frac{M_\odot}{pc^2}} \int_{LOS} \rho_g(r) \left(\frac{Z(r)}{Z_\odot} \right) dr. \tag{1}$$

The spectrum of the stellar particle was then reddened using the extinction law of Fluks et al. (1994).

All the spectra of stellar particles from the same pixel were added up to give the integrated absolute spectrum of the pixel, which was then redshifted and dimmed using the redshift z from the models, and calculating the distance modulus $m - M$ according to Carroll et al. (1992):

$$m - M(z) = 5 \log \left(\frac{c}{H_0} (1 + z) \int_0^z [(1 + z')^2 (1 + \Omega_M z') \right.$$
$$\left. - z'(2 + z') \Omega_\Lambda]^{-1/2} dz' \right) + 25. \tag{2}$$

We then corrected the spectra for Lyman line blanketing and Lyman continuum absorption by absorption systems at cosmological distances using the formulae given by Madau (1995) for QSO absorption systems. Finally, apparent HST (WFPC2
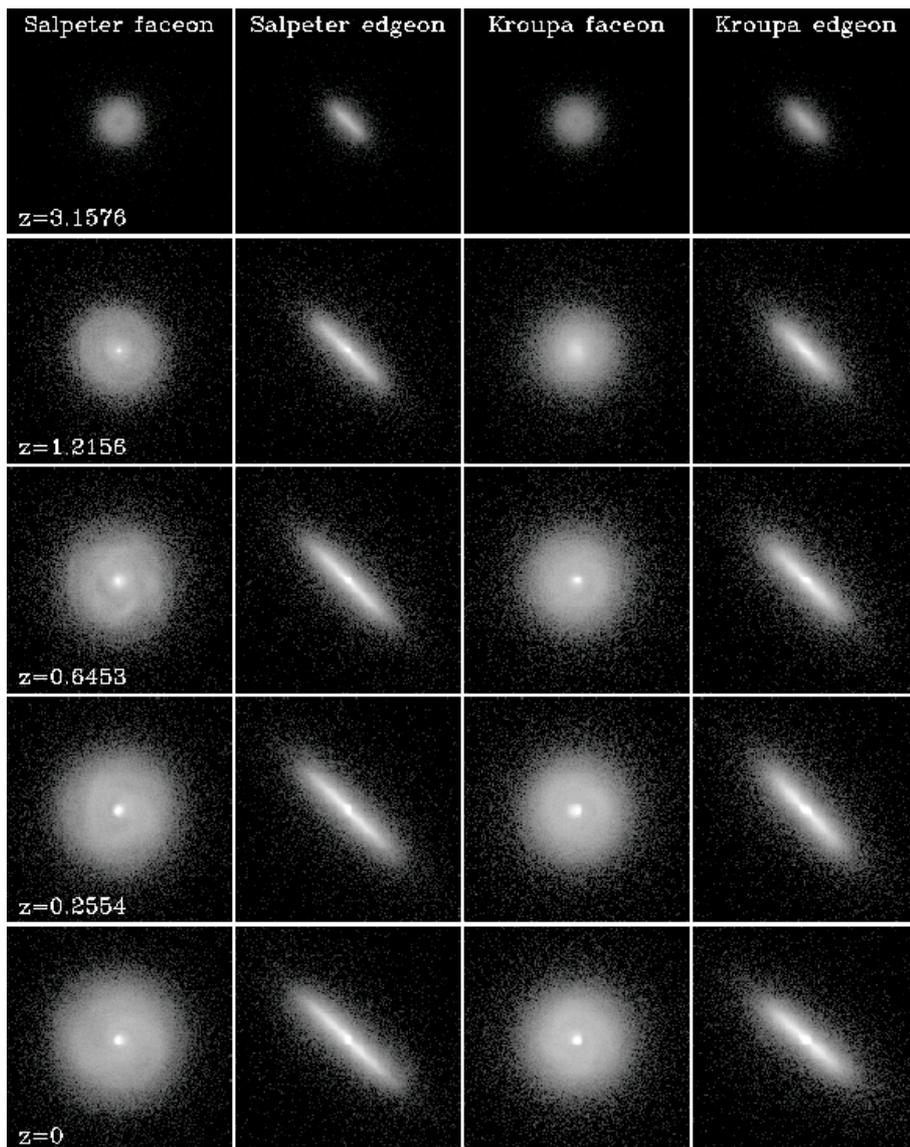
Fig. 3. Stellar mass distributions of the Salpeter and Kroupa models at different redshifts/ages (the redshifts correspond to ages of 2, 5, 7.5, 10.5, and 13.5 Gyr) seen face-on and edge-on. The colour scale is logarithmic and covers four orders of magnitudes. The images show an area of 40 × 40 kpc.

and NICMOS), SDSS *ugriz*, Washington *CNT1T2* colours and magnitudes were calculated for each pixel through synthetic photometry. Other photometric systems, i.e. Johnson-Cousins *UBVRIJHKLM*, Strömgren *ubvy*, Kron *RI*, are also implemented in the programme, but we limited our study to the above-mentioned systems for memory – and CPU time reasons. Including more systems is unlikely to yield further discoveries, since the filter bands of those systems lie in the same wavelength range as the ones of the systems we used, and will thus most probably show the same behaviour with IMF (and other) variations. Furthermore, the HST and SDSS systems seemed most likely to allow extensive comparison with observational data.

At the same time, the absolute (rest frame) spectra and the apparent spectra of all the pixels were added up to derive the absolute and apparent integrated spectra of the galaxy. Examples of such integrated (intrinsic, that is unredshifted and all with the same distance modulus) spectra are shown in Fig. 5. The metallicity-dependent distribution of the stars and the spatially resolved treatment of the gas absorption are the most important for the spectra and colours.

On these integrated spectra, synthetic photometry was performed, too. For computer memory reasons, the spectra of individual pixels or stellar particles were not stored, so the final output quantities of the programme are:

1. a 2-dimensional colour image of the model galaxy, including the effect of internal absorption in intrinsic magnitudes of up to 320 × 320 pixels, as seen from a freely chosen angle,
2. the same image in apparent (redshifted and corrected for the distance modulus and Lyman line blanketing) magnitudes,
3. the integrated intrinsic spectrum of the entire galaxy plus integrated intrinsic colours and absolute magnitudes,
4. the integrated apparent spectrum of the entire galaxy plus integrated redshifted colours and apparent magnitudes.

Our programme also includes the possibility to account for Galactic foreground reddening. But since this option only makes sense for specific applications, where the foreground reddening is known, it was not used in this work.

These quantities were calculated for both the Salpeter IMF and the Kroupa IMF models, at ages from 0.5 Gyr (corresponding to $z = 9.5$, or 0.3 Gyr after the beginning of the simulation) to 13.5 Gyr (the present day) in steps of 0.5 Gyr, and from three different directions: face-on, inclined by 60°, henceforth called the diagonal view, and edge-on. The size of a pixel was chosen to be 0.25 kpc. Higher resolution would make no sense, as the
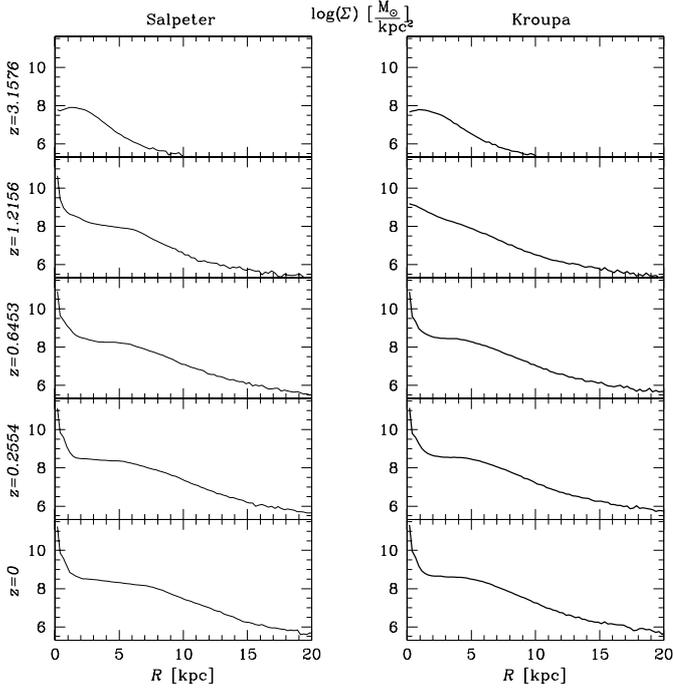
Fig. 4. Stellar (face-on) mass profiles of the Salpeter and Kroupa models at different redshifts/ages. The profiles correspond to the first and third columns of Fig. 3.

galaxy model has a precision of only 0.37 kpc. The entire "camera" was chosen 320×320 pixels wide, thus representing a field of view of 80×80 kpc.

To identify absorption effects, the same photometric properties were calculated for both models without internal absorption. Thus, the differences between the regular models and these ones should reflect absorption effects, or the error in models that do not include internal absorption. These models will be called the absorptionless models, and will be used in Sect. 5.

4. Data extraction

In order to test our models, we compare them to galaxy data from the Sloan Digital Sky Survey (SDSS) (York et al. 2000), which offers a large sample of galaxies. The current volume of the SDSS is the Data Release 4 (DR4) which covers in the imaging mode about 180 million unique objects in an area of 6670 square degrees and 849 920 spectra within 4783 square degrees (Adelman-McCarthy et al. 2005). We use the SDSS Batch Query Services[1] on the DR4 Galaxy Table View and SpecObj Table View. This web interface allows to perform queries on the available SDSS archives using the Structured Query Language (SQL). The Galaxy Table View contains optical parameters of all galaxies at the time of the data release. The spectral properties of the galaxies are given in the SpecObj Table View. We remove all objects which are flagged with one or more of the PhotoFlags as given in the Galaxy Table View: blended (object had multiple peaks detected within it); edge (object is too close to edge of frame of the survey); saturated (object contains saturated pixels); ellipfaint (not measured isophotal properties and incomplete profiles). These flags allow us to reject all objects near the survey borders and blended with spikes of nearby stars. As our model colours differ for the face-on and edge-on

view (see Sect. 5), we extract two samples, one for either viewing direction.

For the edge-on sample, we adopt the query used by Kautsch et al. (2006) to collect a catalog of edge-on galaxies, wherein the axial ratio a/b is chosen to be >3, a and b being the major and minor angular isophotal axes in the g band; the major axis a is chosen larger than 15 pixels (which corresponds to 5.94 arcsec) and colours in the ranges $-0.3 < g - r < 3$ mag and $-0.3 < r - i < 3$ mag, in order to exclude spurious objects and other artefacts. We limit the sample to a Petrosian magnitude[2] in the g band of 20.

For the face-on sample, a/b is chosen to be smaller than 1.5, the isophotal major axis a is also >15 pixels, and the colours again lie in the ranges $-0.3 < g - r < 3$ mag and $-0.3 < r - i < 3$ mag. Here the Petrosian g band magnitude is limited to 19 mag, since galaxies seen face-on appear brighter than the same ones seen edge-on (see Sect. 5). Using these limiting magnitudes, the two samples contain a similar number of galaxies.

The following biases affect our selection: "Shredded galaxies," i.e., these galaxies are detected as two or more independent objects (this is found in particular for extended objects with substructure and diameters $\geqslant 1'$); galaxies with unusual colours caused by an AGN and/or dust. Due to these effects we lose less than 1% of the targets from the SDSS database as estimated from a by-eye-inspection of randomly selected subsamples.

Wrong classification can be the result of various causes: (i) "inverse shredding", where objects arranged in chains are detected as a single object; (ii) bars or spiral arms in faint disks being classified as edge-on galaxies. However, we estimate that these effects affect about 2% of the targets only.

5. Results

In Fig. 6, we see the calculated intrinsic urz band images of the Salpeter and Kroupa model galaxies, both in the same magnitude scaling. The images confirm that the bulge forms later in the Kroupa model (at around 6 Gyr) than in the Salpeter model (~4 Gyr), as mentioned in Sect. 2. Apart from that, the images of the models look extremely similar. In this section, we will explain why.

5.1. Intrinsic magnitudes and mass-to-light ratios

In Tables A.1 to A.4 are listed the intrinsic bolometric, V Johnson, SDSS $ugriz$, and HST (WFPC2 and NICMOS) magnitudes of the two models integrated over the full galaxies in the diagonal view. We calculated the Washington magnitudes as well, and they can also be calculated for other colour systems, such as Johnson-Cousins $UBVRIJHKLM$, Strömgren $ubvy$, and Kron RI. The evolution of the magnitudes show some oscillations around their mean tendencies, which are the result of shadowing of the bulge by dense streams of infalling molecular gas. They only show up in the diagonal view when absorption is included. One should keep in mind that this can be an additional source of scatter when looking at observed magnitudes and colours of galaxies.

---

[1] http://casjobs.sdss.org/CasJobs/default.aspx

[2] The Petrosian magnitudes are derived from the Petrosian flux using a circular aperture centered on every object. The advantage of this method is that this allows an unbiased measurement of a constant fraction of the total galaxy light using the technique based on that of Petrosian (1976). For a detailed description of the Petrosian parameters used in the SDSS we refer to Blanton et al. (2001) and Yasuda et al. (2001).
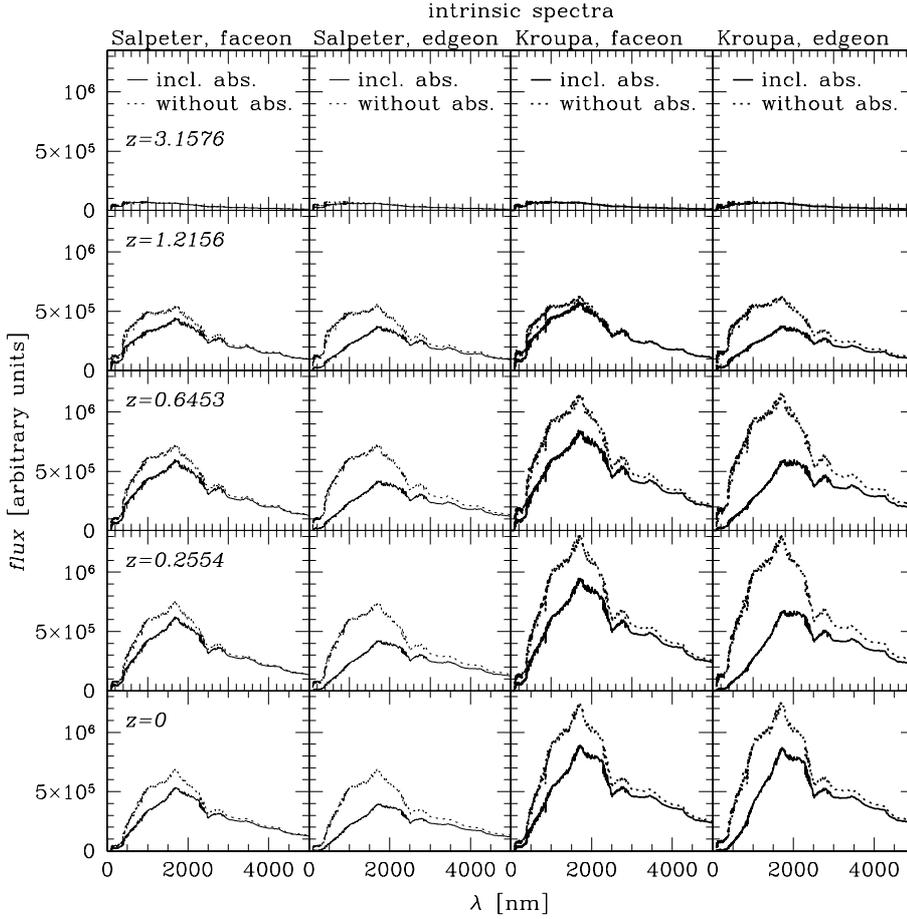
Fig. 5. Intrinsic spectra of the Salpeter (*left two columns*) – and Kroupa (*right two columns*) models at five different epochs (different rows), both face-on (Cols. 1 and 3) and edge-on (Cols. 2 and 4), and both without (dotted) and including (solid) absorption.

In the following, most figures concerning magnitudes will show the SDSS u band and the HST NICMOS $K222$ band, and most figures concerning colours will show $u - g$ and $J110 - K222$, which are the bluest and reddest calculated magnitudes and colours, respectively, and therefore are the most illustrative of the range of possible effects on colours and magnitudes. For other passbands and colours, the trends will usually lie between the trends of the ones shown in the figures.

Tables B.1 to B.4 give the stellar mass-to-light ratios (M/L) of the two models both including and omitting absorption, in bolometric light, Johnson Vj, the SDSS $ugriz$ system, and the HST NICMOS JHK system. They are shown in Fig. 7 in u, r, i, and $K222$ as a function of time since the Big Bang. We see that, from around 6 Gyr on, the Kroupa model has M/Ls about one third lower than the Salpeter model. It is ~0.5 mag brighter, due to its higher SFR (see Fig. 1). Unfortunately, when absorption is included, this effect is partly canceled out by the higher gas content of the Kroupa model to a level varying between 0 ($K222$) and 0.4 mag (u), which is probably undetectable. The effect in colour bands bluewards of i is, that the two models become indistinguishable, an unfortunate coincidence we call "IMF degeneracy". It is weakest in the $K222$ band, where the absorption is smaller and the difference between the Salpeter – and Kroupa models remains around ~0.5 mag, leaving the difference in M/L unaltered, but even this will be difficult to measure.

The above-mentioned absorption effects vary with the viewing angle, as is illustrated for the Kroupa model in Fig. 8 (for the Salpeter model they look similar). It shows the u – and $K222$ evolution of the model in all angles, as well as the absorptionless model (which has the same intrinsic magnitudes viewed

from any angle). The lower panels show the absorption effects on these magnitudes (that is the differences between the models with different viewing angles and their absorptionless counterparts). These differences translate into differences in magnitudes between the different inclinations. They amount to 1.5 mag in u, and still 0.5 mag in $K222$, which is more than the IMF effects. Nevertheless, it will be difficult to say something about the orientation of an unresolved galaxy by its intrinsic magnitude alone, since too many things can affect the total magnitude of a real distant galaxy, besides inclination.

5.2. Intrinsic colours

If IMF effects on magnitudes or Mass-to-light ratios are insignificant, suffering from a degeneracy, does the IMF manifest itself more strongly in the colours? In Fig. 9, top panel, we see the time evolution of $(u - g)_0$ and $(J110 - K222)_0$ of both the Salpeter (thick) – and the Kroupa (thin) models, including absorption (solid) and without (dashed). The bottom panel shows the differences in these colours between the two models, both including absorption (solid) and without (dashed). The thin dotted line shows zero level.

For the $(u - g)_0$ colour, we see the same conspiracy between SFR and absorption as before. The colour difference in unabsorbed starlight between the two models (bottom left panel dashed line), which was already very small from the beginning (below 0.1 mag), is even diminished by the absorption. In $(J110 - K222)_0$, on the other hand, the differences between the Salpeter – and the Kroupa models increase when absorption is taken into account, but they remain too small to be measured
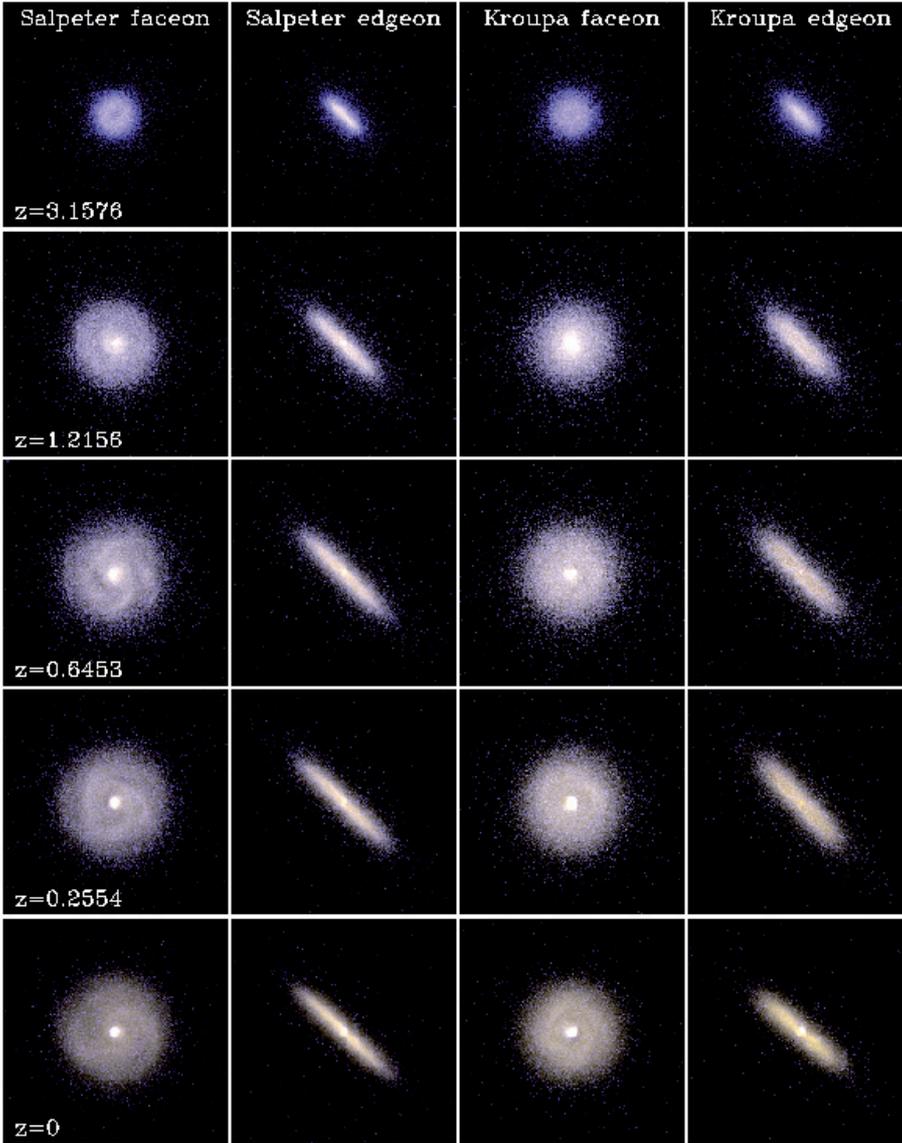
Fig. 6. Calculated intrinsic *urz* images of the Salpeter and Kroupa models, face-on and edge-on, both in the same magnitude scaling, where the calculated *u* distribution makes up for the blue portion of the composite image, the *r* distribution for the yellow portion, and the *z* distribution for the red portion. The images correspond to the images in Fig. 3.

(only up to 0.2 mag). In colours made up of two magnitudes from widely separated wavelength regions, such as $(u - K222)_0$, they even reach 0.5 mag, but in relation to the larger variation of these colours, these differences are less expressive than the 0.2 mag in $(J - K)_0$.

In Fig. 10, we see the effect of reddening on the bluest and the reddest colours of our study, $(u - g)_0$ and $(J110 - K222)_0$, respectively. The top panels show the time evolution of these two colours for the Kroupa model in all three viewing angles, as well as the absorptionless case, which is the same for all viewing angles. The bottom panel shows the differences between the absorbed and the unabsorbed models in all three inclinations. Clearly, the absorption effects on the bluest colours are small, only up to ~0.2 mag in $(u - g)_0$. In $(J110 - K222)_0$, on the other hand, they reach up to 0.8 mag (edge-on), so this colour might be suitable to detect orientation effects. It may seem counter-intuitive, that inclination-induced reddening on the bluest colour is much smaller than in the near infrared. This must be because the differential extinction in $J110$ vs. $K222$ is much larger than in u vs. g.

Having calculated galactic models both omitting dust effects and, as a novelty, self-consistently including them, gives us the unique occasion to test the usual assumption that the combined absorption and reddening effects do not significantly alter colour-M/L relations (Bell & de Jong 2001). Figure 11 shows four such relations, combining colours and M/L ratios from the reddest and the bluest wavelength regions of our calculations. For the relations involving the $(u - g)_0$ colour (left panels), the assumption works reasonably well. The dust effects move the colours and the M/L ratios along the main relations, thereby keeping them in place. For the relations involving $J110 - K222$ (right panels), on the other hand, the colour-M/L relations are shifted by around 0.2 mag to the red, when absorption is included (The dust affects this colour much more than the M/L ratios). It seems difficult to keep these relations intact by altering the colour and the M/L ratios at the same time, since they are not linear in the first place. A systematic investigation shows, that the assumption can be used for colours involving passbands bluewards of the SDSS *i* band.

5.3. Apparent magnitudes

In practice, apparent magnitudes (redshifted and corrected for distance) are more relevant than intrinsic magnitudes, as they are the quantities that are actually observed. They are given in Tables A.5 to A.8 for the same bands as in Tables A.1 to A.4.
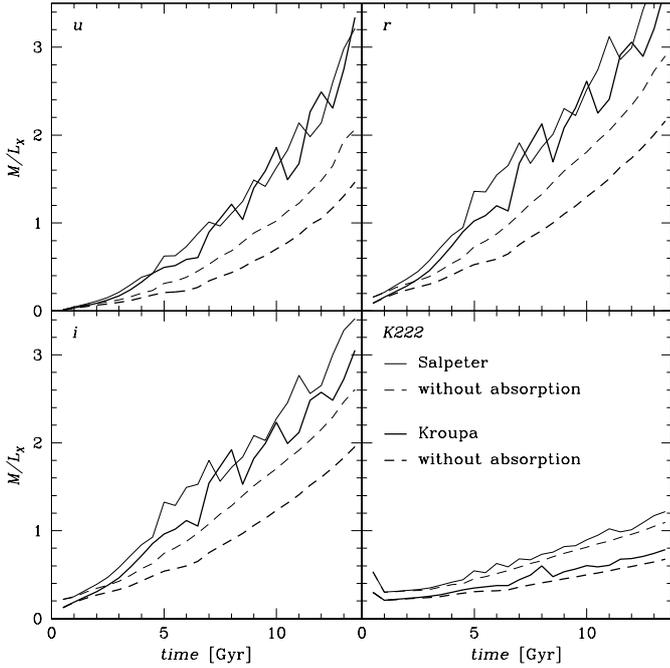
Fig. 7. Stellar mass-to-light ratio evolution in u, r, i, and $K222$ of the Salpeter (thin) and the Kroupa (thick) models, both including (solid) and omitting (dashed) gas absorption.

Due to the very low fluxes at the highest redshift (9.5116, corresponding to a Universe age of 0.5 Gyr), the calculation of the magnitudes at this age suffers too much from precision errors, so these values should be taken with a grain of salt, especially in the bluer passbands. In the bluest bands (u, g, $U336$, and $B439$), the errors might even affect the second time step (redshift 5.6177) as well, especially when combining the magnitudes to calculate colours, on which small differences have a much more dramatic effect than on magnitudes.

For the u and $K222$ bands, the redshift evolution is shown in the top panels of Fig. 13, again for both models in the diagonal view, and both including – and not including absorption, like in the first and fourth panels of Fig. 7. In the bottom panels, we see the differences between the Kroupa and the Salpeter models. These differences between the two models show the same tendencies as for the intrinsic magnitudes (~0.5 in the absorptionless case, reduced when absorption is included), and are probably even harder to detect than they would be in the intrinsic magnitudes, since they are dominated by distance modulus effects. Again, the $K222$ band is slightly better for detecting the differences (they remain around 0.5 mag even after including absorption) than the SLOAN filters, but still not good enough.

The absorption effects on the Kroupa model, that is the magnitude differences between the absorptionless and the absorbed model, are given in all calculated passbands in Tables C.1 and C.2 for the diagonal view. Together with the inclination corrections given in Tables C.3 to C.6, they can be calculated for all three viewing angles. By subtracting the inclination or absorption corrections for two magnitudes, the inclination or absorption (reddening) corrections for the corresponding colour can be derived. This can be useful to make absorption corrections to galactic models. We only give these corrections for the Kroupa model, because this model is more realistic, and the corrections are very similar for the Salpeter model. As expected, the absorption is the strongest in the edge-on view and the weakest face-on, but the latter does not differ much from the diagonal case.
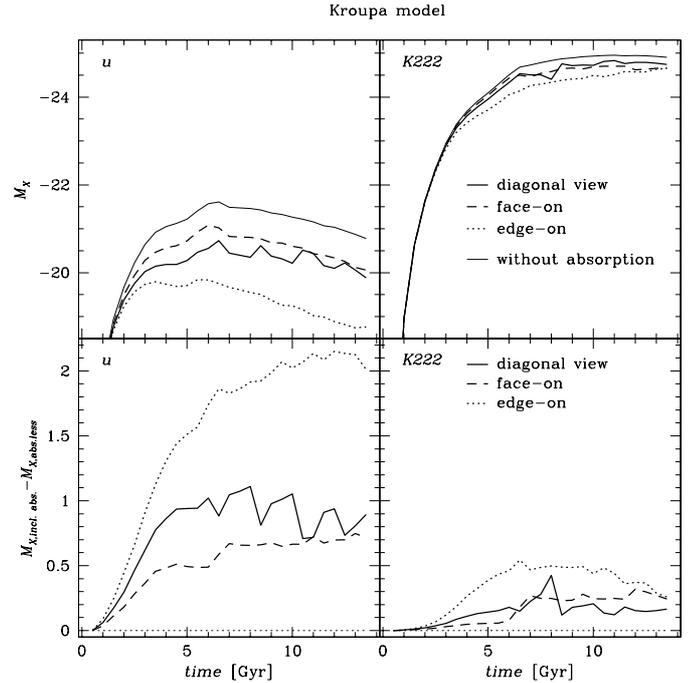
Fig. 8. *Top panels*: absolute u and $K222$ magnitude evolution of the Kroupa model as seen in the diagonal view (solid), face-on (dashed), and edge-on (dotted). The thin solid line shows the evolution of the absorptionless model (in the diagonal view, but it looks the same for the face-on and edge-on views). *Bottom panels*: effects of the gas absorption on the absolute u and $K222$ magnitudes of the Kroupa models (that is, the differences between the absorptionless and the regular models) as seen in the diagonal view (solid), face-on (dashed), and edge-on (dotted). The thin dotted lines show the zero level.

Fig. 9. *Top panels*: intrinsic $(u-g)_0$ and $(J110-K222)_0$ colour evolution of the Salpeter (thin) and the Kroupa (thick) models, both including (solid) and omitting (dashed) gas absorption. *Bottom panel*: differences in 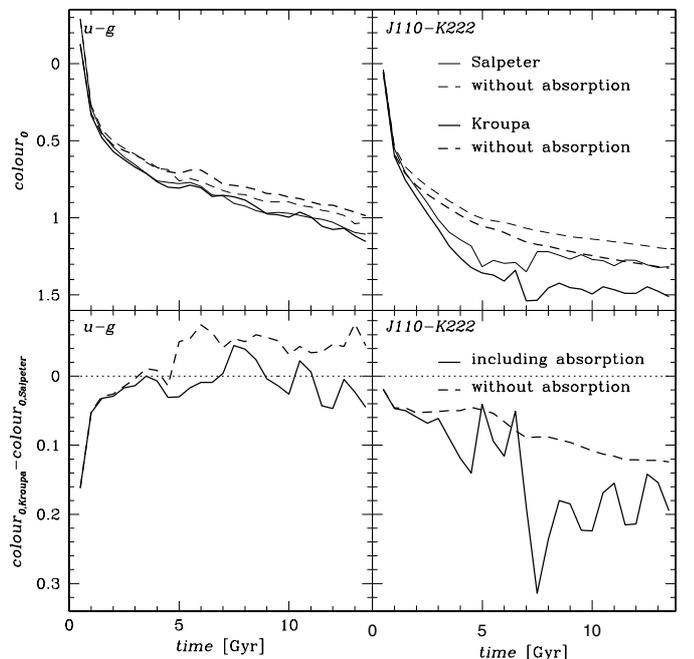intrinsic $(u-g)_0$ and $(J110-K222)_0$ colours between the Salpeter and the Kroupa models, both including (solid) and omitting (dashed) gas absorption. The thin dotted line shows the zero level.
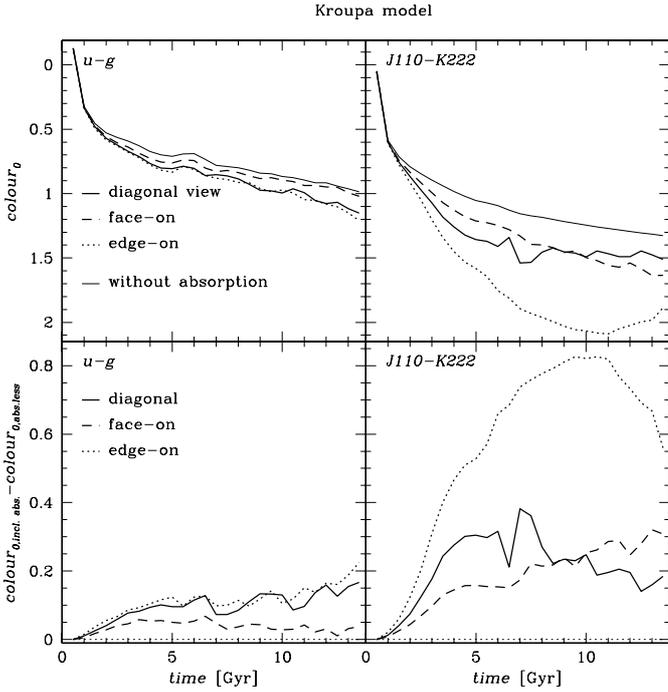
Fig. 10. *Top panels*: intrinsic $(u - g)_0$ and $(J110 - K222)_0$ colour evolution of the Kroupa model as seen in the diagonal view (solid), face-on (dashed), and edge-on (dotted). The thin solid line shows the evolution of the absorptionless model (in the diagonal view, but it looks the same for the face-on and edge-on views). *Bottom panels*: absorption effects on the intrinsic $(u - g)_0$ and $(J110 - K222)_0$ colours of the Kroupa models in each of the three viewing directions, that is, the differences between the absorbed and the absorptionless model seen in the diagonal view (solid), face-on (dashed), and edge-on (dotted). The thin dotted lines show the zero level.

So even for face-on galaxies, it will be impossible to infer the IMF from an integrated magnitude, whereas for edge-on galaxies, the situation is even worse.

If the apparent magnitudes calculated from the models cannot be used to discriminate between the two different IMFs, do they at least reproduce the empirical data? In order to compare our model magnitudes with those from Sect. 4 that represent similar galaxies as in our models, we reduced both data sets (edge-on and face-on) to those galaxies with similar sizes (Petrosian radii) and structure (concentration indices) as the model galaxies. Ideally, one should compare the models to galaxies with the same mass and morphological type, but since these quantities are not given in the SDSS, we resort to size and concentration parameters. More precisely, we determined petroR90$_r$ and C$_r$ as a function of redshift z for both the Salpeter and the Kroupa models, face-on and edge-on, and then reduced the data sets to those galaxies that fulfilled the following criterion:

$$0.5 \cdot \text{petroR90}_{r,\text{mod}}(z) < \text{petroR90}_{r,\text{emp}}(z)$$

$$< 2.0 \cdot \text{petroR90}_{r,\text{mod}}(z) \wedge$$

$$0.98 \cdot C_{r,\text{mod}}(z) < C_{r,\text{emp}}(z) < 1.02 \cdot C_{r,\text{mod}}(z) \quad (3)$$

where petroR90$_{r,\text{mod}}(z)$ and C$_{r,\text{mod}}(z)$ are the Petrosian radius and concentration index calculated from the models and petroR90$_{r,\text{emp}}(z)$ and C$_{r,\text{emp}}(z)$ are the values taken from the SDSS data base, as well as the redshift z. The calculated Petrosian radii (both in kpc and in arcsec) and concentration
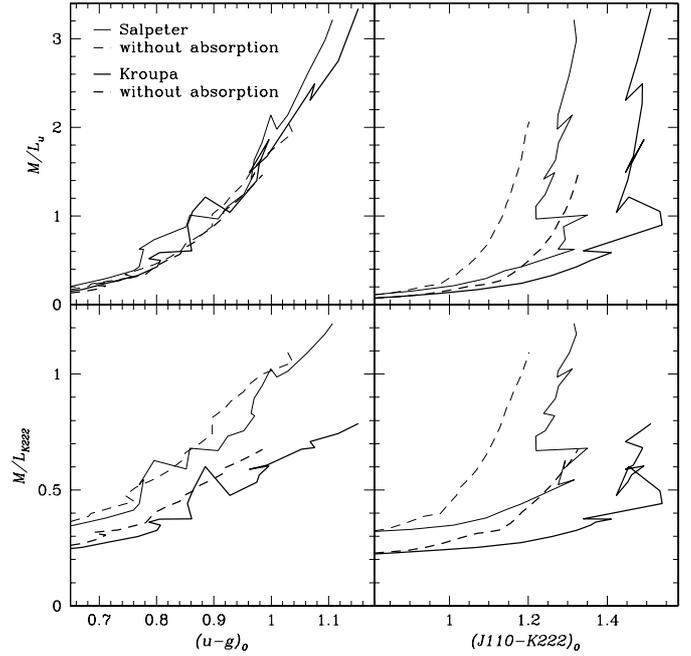
Fig. 11. Colour-M/L relations of the two models in different passbands, including and omitting absorption.

indices are given for the Kroupa model in Tables D.1 to D.3, as they could be useful to identify Milky Way-type galaxies or progenitors at high redshift. At the first time step (0.5 Gyr, redshift 9.5116), however, these values still suffer from the initial border conditions of the model, and cannot be used. The concentration indices could only be calculated from redshift 1.5915 on.

The apparent u band magnitudes including their error bars of the subsamples are plotted as a function of redshift in Fig. 14. The thick dashed and dotted lines show the evolution of the corresponding models (dashed: face-on, dotted: edge-on). The thin lines show the respective other views for the same models (thus the thick lines in the upper panels correspond to the thin lines in the lower panels, and vice-versa), to show the differences in brightness between the two viewing angles. The models are only shown until the second-last time step at redshift 0.0369, as the magnitudes at redshift 0 depend on the actual distance, which is unknown. The distance modulus $m - M$ of 25 used in Tables A.5 to A.8 is only a convention, whereas in reality the distance modulus at zero redshift depends upon the actual distance and Eq. (2) is not valid.

As can be seen from Fig. 14, the models represent the u magnitudes of the empirical samples well, and they even reproduce the brightness differences between the face-on and the edge-on views.

Figure 15 shows the same galaxies and models as Fig. 14, but in the r band. Here too, the agreement is good, although one could argue that the magnitudes of the Salpeter model are a bit too faint.

5.4. Apparent colours

Let us move on to apparent colours. Figure 16 shows the redshift evolution of apparent $u - g$ and $J110 - K222$, the different line types and widths having the same meaning as in Fig. 13. The figure is only shown out to redshift 5.9, due to the above-mentioned imprecisions at redshift 9.5116. In $u - g$, they might even affect the data point at redshift 5.6177. In $u - g$, we again see our "IMF
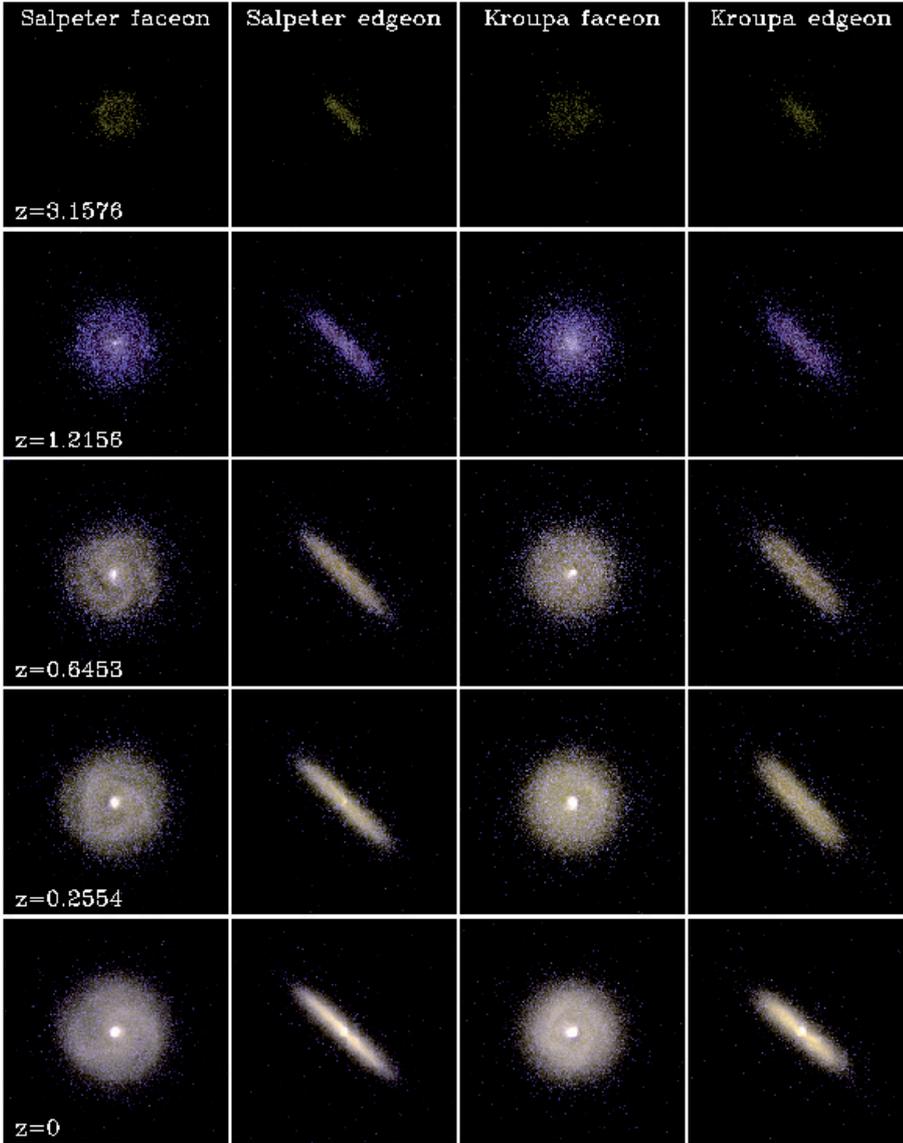
Fig. 12. Calculated apparent *urz* images of the Salpeter and Kroupa models, face-on and edge-on, both in the same magnitude scaling (corrected for distance modulus), where the calculated *u* distribution makes up for the blue portion of the composite image, the *r* distribution for the yellow portion, and the *z* distribution for the red portion. The images correspond to the images in Fig. 3.

degeneracy", the fact that the higher absorption in the Kroupa model compensates the bluer colour caused by the higher SFR. This leaves the $u - g$ differences between the two models at a level of at most 0.05 mag, which is undetectable given the much larger variations this colour shows during the evolution. At best, the differences could be seen in $J110 - K222$, where they amount to ~0.2 mag (edge-on up to 0.4 mag), which is a significant fraction of the variation of this colour after 2.5 Gyr. (~0.7 mag). Let us see how the models compare to the empirical data. In Figs. 17 to 19, we see the $u - g$, $r - i$, and $r - z$ colours of the two models, face-on and edge-on, as a function of redshift in the same coding as in Fig. 14. Overplotted are the colours including error bars of the four subsamples of galaxies selected using Eq. (3), so the models are only compared to data from galaxies of the same types (angular sizes, concentration parameters, and viewing angles).

Obviously, the model colours are too blue by about 0.3 to 0.4 mag in $u - g$, by about 0.1 mag in $r - i$, and more or less in the right colour range for $r - z$. Also, the trends with redshift are not always well reproduced in the latter two colours. This could be an indication, that hierarchical-based accretion histories may induce a delayed galaxy formation, resulting in too blue colours especially at high redshift. It looks like SDSS galaxies on average have an earlier Hubble type star formation history than the Milky Way type model galaxy. This argument is also supported by the fact, that the monolithic collapse model in Westera et al. (2002b) produces colours in better agreement with the data. In spite of these systematic deviations, the models do seem to reproduce relative properties, i.e. the effect of galaxy orientation on integrated colours, as can be seen from the fact, that they nicely reproduce the shift between face-on – and edge-on colours, thereby underlining the usefulness of the corrections given in Tables C.1 to C.6. This is why we believe that the results we found comparing the models with different IMFs are also realistic. We thus conclude that it is difficult to make statements about the stellar IMF from integrated colours or magnitudes of galaxies. Our best bet for this purpose are infrared colours, i.e. $J110 - K222$.

6. Summary and conclusions

In this work, we use chemo-dynamical models to investigate the influence of the Initial Mass Function (IMF) on the evolution of a Milky Way-type disk galaxy, in particular of its colours.

For this purpose, we developed two chemodynamical models of such a galaxy with the same boundary conditions, but using
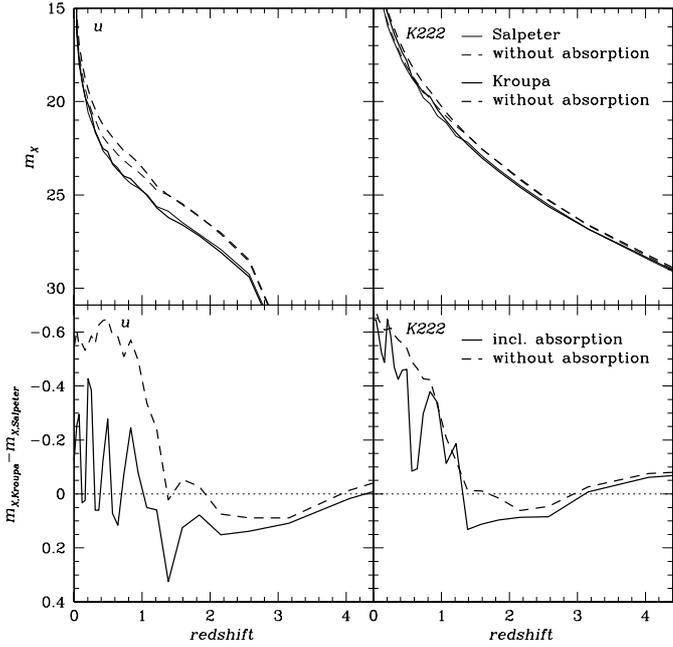
Fig. 13. *Top panels*: apparent u and $K222$ magnitude evolution of the Salpeter (thin) and the Kroupa (thick) models as a function of redshift, both including (solid) and omitting (dashed) gas absorption. *Bottom panels*: differences in u and $K222$ magnitudes between the Salpeter and the Kroupa models, both including (solid) and omitting (dashed) gas absorption. The thin dotted lines show the zero level.
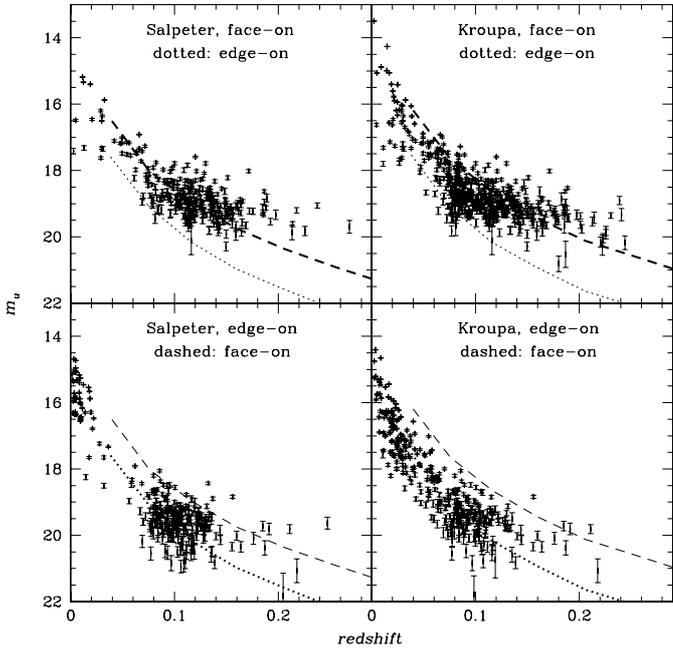

Fig. 14. Apparent u magnitudes of the Salpeter and Kroupa models as seen face-on (dashed) and edge-on (dotted) as a function of redshift. Overlaid are the SDSS DR4 data with their observational errors of galaxies that have similar sizes, concentration parameters, and orientation as the models (for a more precise description, see the text).

different IMFs: Salpeter and Kroupa, which differ in their low-to-high mass stars ratios. The Kroupa model, having a higher fraction of high mass stars, begins with a lower SFR than the Salpeter model, but from 5 Gyr on, this reverses. The Kroupa model also has a higher gas density and metallicity than the Salpeter model at all ages.
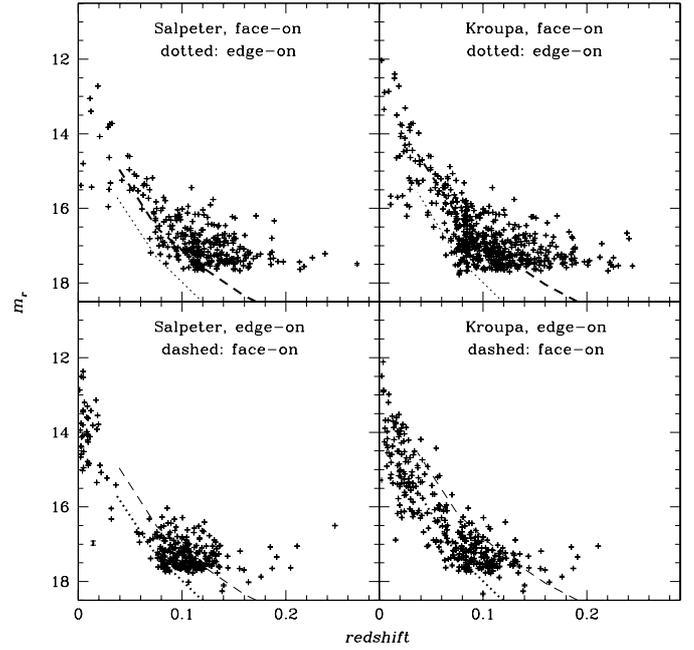
Fig. 15. Like Fig. 14, but for the r band.
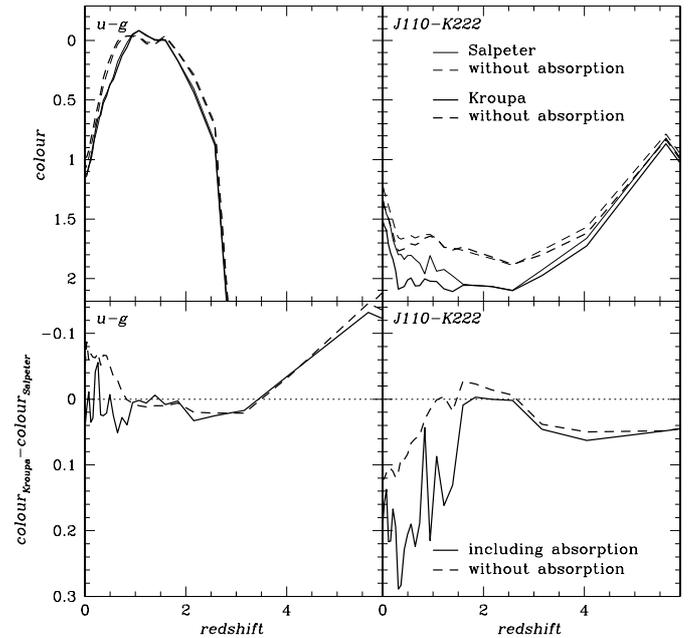
Fig. 16. *Top panels*: apparent $u - g$ and $J110 - K222$ colour evolution of the Salpeter (thin) and the Kroupa (thick) models as a function of redshift, both including (solid) and omitting (dashed) gas absorption. *Bottom panels*: differences in the $u-g$ and $J110-K222$ colours between the Salpeter and the Kroupa models, both including (solid) and omitting (dashed) gas absorption. The thin dotted lines show the zero level.

With these two models, we performed a spectral analysis, evaluated with a state of the art evolutionary code and spectral library. The programme transforming the models into spectral properties takes into account the three-dimensional distribution of the stars and the interstellar matter. It includes internal gas absorption and re-emission and is also able to include foreground reddening. We obtain two-dimensional HST (WFPC2 and NICMOS), and SDSS *ugriz* images of the model galaxies, giving intrinsic and apparent magnitudes and colours in up to 320×320 pixels. We also obtain intrinsic and apparent
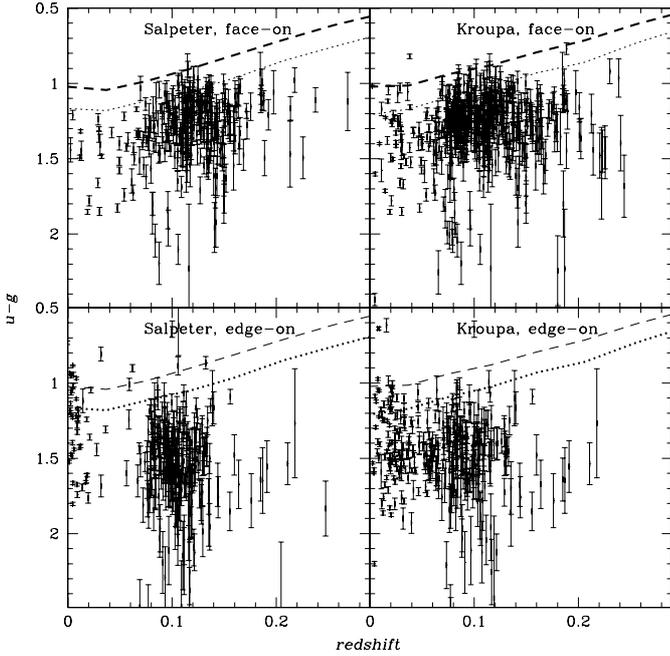
Fig. 17. Apparent $u - g$ colours of the Salpeter and Kroupa models as seen face-on (dashed) and edge-on (dotted) as a function of redshift. Overlaid are the SDSS DR4 data with their observational errors of galaxies that have similar sizes, concentration parameters, and orientation as the models (for a more precise description, see the text).
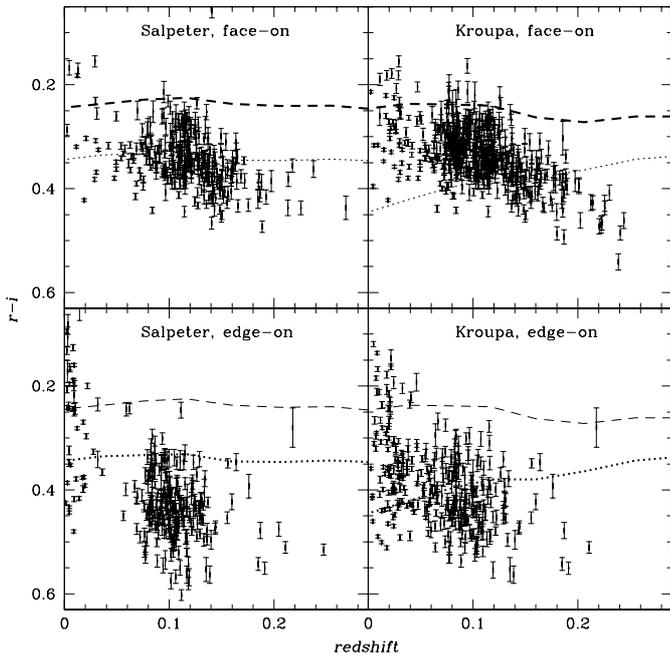
Fig. 18. Like Fig. 17, but for $r - i$.

integrated spectra and colours of the model galaxies. All of these quantities were calculated with a time resolution of 0.5 Gyr. The programme is able to view the model galaxies from different angles (diagonally, face-on, and edge-on), which allows to analyse orientation effects on the spectral properties. Furthermore, by recalculating the models artificially omitting the gas absorption, we could disentangle absorption effects from other effects. We provide photometric absorption and inclination corrections
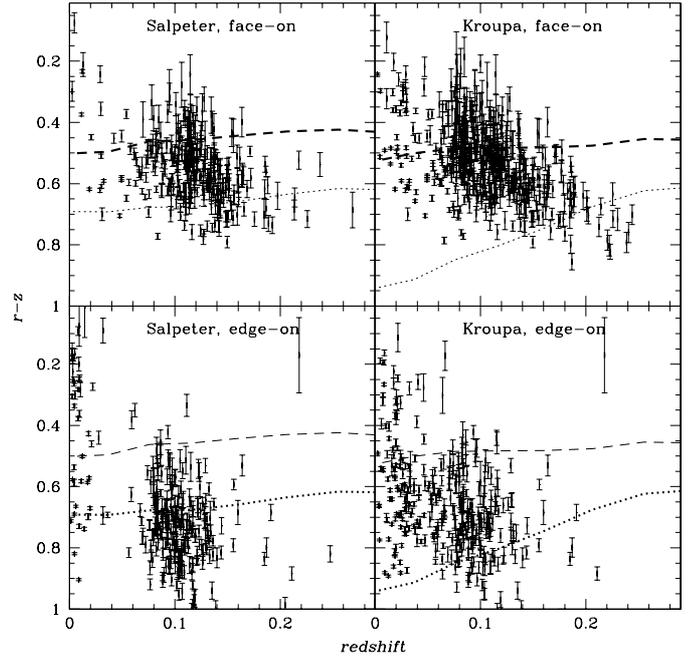
Fig. 19. Like Fig. 17, but for $r - z$.

in the SDSS *ugriz* and the HST WFPC2 and NICMOS systems (Tables C.1 to C.6).

We find, that the effect of the IMF on the internal gas absorption is larger than its effect on the light from the stellar content. However, the two effects work in the opposite sense (An IMF with more high mass stars leads to brighter and bluer stellar light, but also to more interstellar dust and thus to more absorption), causing a kind of "IMF degeneracy". The most likely wavelength region, in which to detect IMF effects is the infrared (i.e. *JHK*). Here, the differences between the two models amount to ~0.5 mag in $K222$, and to ~0.2 mag in $J110 - K222$.

The effects of inclination on a galaxy's magnitudes and colours, on the other hand, are larger than the ones due to the IMF. Seeing a galaxy edge-on instead of face-on or diagonally can make it appear up to 1.5 mag fainter in *u*, or 1 mag in *z*, or 0.6 mag redder in $J110 - K222$.

A comparison of the calculated integrated model magnitudes and colours with SDSS data partly shows good agreement, especially in the *u* and *g* magnitudes, and the *riz* colours. There are some systematic deviations in the UV colours, indicating that SDSS galaxies might have on average an earlier Hubble type star formation history than the model galaxy, which is more like the Milky Way. On the other hand, the relative tendencies in these colours are well reproduced (i.e. the shift between face-on and edge-on colours of galaxies of the same type). We conclude from this, that the theoretical results presented in the two previous paragraphs should hold true in practice as well.

As a side study, we verify the assumption by Bell & de Jong (2001), that the combined absorption and reddening effects of dust do not significantly alter the colour-M/L relations for galaxy models, and find this assumption only to be true for colours involving passbands in the bluer wavelength ranges (bluewards of the *I* band).

References

Adelman-McCarthy, J. K., et al. 2005, ApJS, 162, 38
Barnes, J., & Efstathiou, G. 1987, ApJ, 319, 575
Bell, E. F., & de Jong, R. S. 2001, ApJ, 550, 212
Blanton, M. R., Dalcanton, J., Eisenstein, D., et al. 2001, AJ, 121, 2358
Bruzual, A. G., & Charlot, S. 1993, ApJ, 405, 538
Bruzual, A. G., & Charlot, S. 2003, MNRAS, 344, 1000
Bullock, J. S., Dekel, A., Kolatt, T. S., et al. 2001, ApJ, 555, 240
Carigi, L., Colín, P., & Peimbert, M. 1999, ApJ, 514, 787
Carroll, S. M., Press, W. H., & Turner, E. L. 1992, ARA&A, 30, 499
Chabrier, G. 2001, ApJ, 554, 1274
Chabrier, G. 2002, ApJ, 567, 304
Chabrier, G. 2003, PASP, 115, 763
Charlot, S., & Bruzual, A. G. 1991, ApJ, 367, 126
Eggen, O. J., Lynden-Bell, D., & Sandage, A. R. 1962, ApJ, 136, 748
Fagotto, F., Bressan, A., Bertelli, G., & Chiosi, C. 1994, A&AS, 105, 39
Ferraro, F. R., Carretta, E., Bragaglia, A., Renzini, A., & Ortolani, S. 1997, MNRAS, 286, 1012
Fluks, M. A., Plez, B., The, P. S., et al. 1994, A&AS, 105, 311
Girardi, L., Bressan, A., Chiosi, C., Bertelli, G., & Nasi, E. 1996, A&AS, 117, 113
Girardi, L., Bressan, A., Bertelli, G., & Chiosi, C. 2000, A&AS, 141, 371, Padova 2000, isochrones
Gould, A., Bahcall, J. N., & Flynn, C. 1997, ApJ, 482, 913
Gould, A., Flynn, C., & Bahcall, J. N. 1998, ApJ, 503, 798
Kautsch, S. J., Grebel, E. K., Barazza, F. D., & Gallagher, J. S., III 2006, A&A, 445, 765
Kennicutt, R. C. 1983, ApJ, 272, 54
Kroupa, P. 1998, The Stellar Mass Function (invited review) in Brown Dwarfs and Extrasolar Planets, ed. R. Rebolo, L. Eduardo Martin, & M. R. Zapatero Osorio (San Francisco: ASP), ASP Conf. Ser., 134, 483
Kroupa, P. 2001, MNRAS, 322, 231
Kroupa, P. 2002, Science, 295, 82
Kroupa, P., Tout, C. A., & Gilmore, G. 1993, MNRAS, 262, 545

Larson, R. B. 1998, MNRAS, 301, 569
Leitherer, C., Schaerer, D., Goldader, J. D., et al. 1999, ApJS, 123, 3
Lequeux, J. 1979, A&AS, 80, 35
Lerner, M. S., Sundin, M., & Thomasson, M. 1999, A&A, 344, 483
Madau, P. 1995, ApJ, 441, 18
Miller, G. E., & Scalo, J. M. 1979, ApJS, 41, 513
Petrosian, V. 1976, ApJ, 209, L1
Piotto, G., Cool, A. M., & King, I. R. 1997, AJ, 113, 1345
Piotto, G., & Zoccali, M. 1999, A&A, 345, 485
Portinari, L., Sommer-Larsen, J., & Tantalo, R. 2004, MNRAS, 347, 691
Quillen, A. C., & Yukita, M. 2001, AJ, 121, 2095
Reid, I. N., & Gizis, J. E. 1997, AJ, 113, 2246
Salpeter, E. E. 1955, ApJ, 121, 161
Samland, M., & Gerhard, O. E. 2003, A&A, 399, 961
Scalo, J. M. 1986, The initial mass function of massive stars in galaxies Empirical evidence, in Luminous Stars and Associations in Galaxies, IAU Symp., 116, 451
Scalo, J. M. 1998, The IMF Revisited: A Case for Variations, in The Stellar Initial Mass Function, 38th Herstmonceux Conference, ed. G. Gilmore, & D. Howell (San Francisco: ASP), ASP Conf. Ser., 142, 201
Stephens, A. W., Frogel, J. A., Ortolani, S., et al. 2000, AJ, 119, 419
van den Bosch, F. C. 2002, MNRAS, 331, 98
Wechsler, R. H., Bullock, J. S., Primack, J. R., Kravtsov, A. V., & Dekel, A. 2002, ApJ, 568, 52
Westera, P. 2001, The BaSeL 3.1 models: Metallicity calibration of a theoretical stellar spectral library and its application to chemo-dynamical galaxy models, Ph.D. Thesis, Univ. of Basel, 378
Westera, P., Lejeune, T., Buser, R., Cuisinier, F., & Bruzual, A. G. 2002a, A&A, 381, 524
Westera, P., Samland, M., Buser, R., & Gerhard, O. E. 2002b, A&A, 389, 761
Wilkinson, M. I., & Evans, M. W. 1999, MNRAS, 310, 645
Yasuda, N., Fukugita, M., Narayanan, V. K., et al. 2001, AJ, 122, 1104
York, D. G., Adelman, J., Anderson, J. E., Jr., et al. 2000, AJ, 120, 1579
Zoccali, M., Cassisi, S., Frogel, J. A., et al. 2000, ApJ, 530, 418

Online Material

Appendix A: Intrinsic magnitudes

Table A.1. Intrinsic integrated SDSS magnitudes of the Salpeter model.

t[Gyr]	M_{Bol}	M_{V_j}	M_u	M_g	M_r	M_i	M_z
0.5	−15.586	−12.621	−13.207	−12.918	−12.430	−12.171	−11.957
1.0	−19.467	−17.749	−17.563	−17.844	−17.706	−17.643	−17.583
1.5	−20.513	−19.160	−18.736	−19.187	−19.157	−19.147	−19.141
2.0	−21.132	−19.964	−19.403	−19.944	−19.986	−20.013	−20.047
2.5	−21.562	−20.505	−19.843	−20.449	−20.548	−20.609	−20.682
3.0	−21.848	−20.855	−20.114	−20.770	−20.916	−21.008	−21.117
3.5	−22.004	−21.067	−20.242	−20.954	−21.145	−21.261	−21.397
4.0	−22.095	−21.208	−20.310	−21.070	−21.301	−21.437	−21.590
4.5	−22.265	−21.389	−20.478	−21.248	−21.482	−21.614	−21.764
5.0	−22.113	−21.211	−20.286	−21.063	−21.309	−21.447	−21.603
5.5	−22.332	−21.388	−20.461	−21.231	−21.496	−21.659	−21.849
6.0	−22.292	−21.411	−20.456	−21.252	−21.516	−21.662	−21.824
6.5	−22.329	−21.444	−20.394	−21.246	−21.578	−21.774	−21.991
7.0	−22.266	−21.404	−20.352	−21.210	−21.530	−21.707	−21.898
7.5	−22.436	−21.621	−20.496	−21.403	−21.764	−21.952	−22.148
8.0	−22.384	−21.584	−20.428	−21.352	−21.735	−21.933	−22.135
8.5	−22.361	−21.567	−20.373	−21.325	−21.724	−21.929	−22.139
9.0	−22.270	−21.470	−20.242	−21.213	−21.638	−21.858	−22.083
9.5	−22.367	−21.570	−20.352	−21.317	−21.734	−21.944	−22.160
10.0	−22.288	−21.482	−20.253	−21.223	−21.651	−21.871	−22.095
10.5	−22.242	−21.428	−20.174	−21.158	−21.604	−21.833	−22.066
11.0	−22.143	−21.326	−20.047	−21.046	−21.508	−21.748	−21.990
11.5	−22.264	−21.458	−20.169	−21.179	−21.639	−21.870	−22.106
12.0	−22.242	−21.439	−20.120	−21.149	−21.626	−21.866	−22.109
12.5	−22.112	−21.309	−19.937	−21.000	−21.508	−21.762	−22.019
13.0	−22.022	−21.228	−19.814	−20.908	−21.432	−21.691	−21.949
13.5	−21.989	−21.193	−19.755	−20.862	−21.404	−21.670	−21.935

Table A.2. Intrinsic integrated HST magnitudes of the Salpeter model.

t[Gyr]	M_{U336}	M_{B439}	M_{V555}	M_{V606}	M_{R675}	M_{I814}	M_{J110}	M_{H160}	M_{K222}
0.5	−14.51	−12.94	−12.70	−12.65	−12.59	−12.55	−12.48	−12.49	−12.52
1.0	−18.73	−17.77	−17.77	−17.83	−17.96	−18.10	−18.20	−18.58	−18.75
1.5	−19.86	−19.08	−19.16	−19.26	−19.43	−19.64	−19.80	−20.29	−20.50
2.0	−20.51	−19.81	−19.95	−20.07	−20.28	−20.52	−20.73	−21.30	−21.54
2.5	−20.94	−20.30	−20.49	−20.63	−20.85	−21.14	−21.40	−22.03	−22.30
3.0	−21.20	−20.60	−20.83	−20.99	−21.23	−21.56	−21.86	−22.57	−22.87
3.5	−21.31	−20.77	−21.03	−21.21	−21.47	−21.83	−22.17	−22.93	−23.26
4.0	−21.37	−20.87	−21.17	−21.35	−21.64	−22.01	−22.37	−23.17	−23.51
4.5	−21.55	−21.05	−21.35	−21.53	−21.82	−22.19	−22.55	−23.37	−23.73
5.0	−21.35	−20.86	−21.17	−21.36	−21.65	−22.02	−22.41	−23.29	−23.72
5.5	−21.53	−21.02	−21.34	−21.54	−21.84	−22.26	−22.67	−23.56	−23.95
6.0	−21.52	−21.04	−21.37	−21.56	−21.86	−22.24	−22.62	−23.48	−23.91
6.5	−21.45	−21.01	−21.39	−21.61	−21.94	−22.39	−22.83	−23.73	−24.11
7.0	−21.40	−20.97	−21.35	−21.57	−21.88	−22.30	−22.72	−23.64	−24.07
7.5	−21.54	−21.15	−21.57	−21.79	−22.12	−22.55	−22.96	−23.82	−24.18
8.0	−21.47	−21.09	−21.53	−21.76	−22.10	−22.54	−22.95	−23.80	−24.17
8.5	−21.41	−21.05	−21.51	−21.75	−22.09	−22.54	−22.96	−23.83	−24.20
9.0	−21.27	−20.93	−21.41	−21.65	−22.01	−22.48	−22.91	−23.80	−24.18
9.5	−21.39	−21.04	−21.51	−21.75	−22.10	−22.56	−22.98	−23.85	−24.22
10.0	−21.29	−20.94	−21.42	−21.67	−22.02	−22.49	−22.92	−23.80	−24.19
10.5	−21.21	−20.87	−21.36	−21.62	−21.98	−22.46	−22.90	−23.78	−24.18
11.0	−21.08	−20.75	−21.26	−21.52	−21.89	−22.38	−22.83	−23.73	−24.14
11.5	−21.20	−20.88	−21.39	−21.65	−22.02	−22.50	−22.94	−23.82	−24.21
12.0	−21.15	−20.84	−21.37	−21.63	−22.01	−22.50	−22.95	−23.84	−24.22
12.5	−20.96	−20.68	−21.24	−21.51	−21.90	−22.40	−22.86	−23.77	−24.17
13.0	−20.83	−20.58	−21.15	−21.43	−21.82	−22.33	−22.80	−23.70	−24.12
13.5	−20.77	−20.53	−21.12	−21.40	−21.80	−22.31	−22.78	−23.69	−24.10

Table A.3. Intrinsic integrated SDSS magnitudes of the Kroupa model.

t[Gyr]	M_{Bol}	M_{V_j}	M_u	M_g	M_r	M_i	M_z
0.5	−15.823	−13.180	−13.541	−13.414	−12.994	−12.714	−12.490
1.0	−19.526	−17.907	−17.659	−17.993	−17.839	−17.751	−17.705
1.5	−20.522	−19.227	−18.769	−19.252	−19.203	−19.179	−19.189
2.0	−21.098	−19.968	−19.380	−19.950	−19.975	−19.996	−20.047
2.5	−21.482	−20.434	−19.757	−20.380	−20.466	−20.528	−20.618
3.0	−21.762	−20.777	−20.025	−20.695	−20.830	−20.924	−21.046
3.5	−21.937	−20.966	−20.147	−20.859	−21.039	−21.161	−21.315
4.0	−22.007	−21.083	−20.184	−20.951	−21.173	−21.318	−21.493
4.5	−22.056	−21.145	−20.189	−20.990	−21.252	−21.419	−21.614
5.0	−22.172	−21.249	−20.277	−21.084	−21.364	−21.539	−21.745
5.5	−22.365	−21.417	−20.465	−21.252	−21.533	−21.710	−21.922
6.0	−22.477	−21.530	−20.553	−21.358	−21.652	−21.837	−22.059
6.5	−22.646	−21.780	−20.727	−21.588	−21.913	−22.105	−22.334
7.0	−22.447	−21.497	−20.446	−21.300	−21.635	−21.838	−22.079
7.5	−22.424	−21.474	−20.400	−21.263	−21.622	−21.838	−22.087
8.0	−22.375	−21.460	−20.353	−21.238	−21.614	−21.834	−22.080
8.5	−22.693	−21.789	−20.618	−21.546	−21.958	−22.183	−22.444
9.0	−22.542	−21.630	−20.380	−21.355	−21.819	−22.075	−22.361
9.5	−22.523	−21.582	−20.315	−21.294	−21.781	−22.052	−22.354
10.0	−22.466	−21.508	−20.214	−21.210	−21.714	−21.995	−22.307
10.5	−22.671	−21.747	−20.512	−21.474	−21.936	−22.179	−22.459
11.0	−22.639	−21.719	−20.440	−21.433	−21.916	−22.166	−22.454
11.5	−22.464	−21.535	−20.158	−21.211	−21.755	−22.038	−22.350
12.0	−22.461	−21.514	−20.097	−21.173	−21.745	−22.042	−22.369
12.5	−22.527	−21.619	−20.220	−21.288	−21.842	−22.118	−22.426
13.0	−22.440	−21.529	−20.062	−21.179	−21.763	−22.052	−22.369
13.5	−22.344	−21.405	−19.880	−21.032	−21.652	−21.958	−22.292

Table A.4. Intrinsic integrated HST magnitudes of the Kroupa model.

t[Gyr]	M_{U336}	M_{B439}	M_{V555}	M_{V606}	M_{R675}	M_{I814}	M_{J110}	M_{H160}	M_{K222}
0.5	−14.80	−13.39	−13.24	−13.20	−13.14	−13.09	−13.02	−13.04	−13.07
1.0	−18.82	−17.91	−17.93	−17.98	−18.07	−18.22	−18.35	−18.78	−18.95
1.5	−19.89	−19.14	−19.23	−19.32	−19.47	−19.67	−19.87	−20.41	−20.63
2.0	−20.49	−19.81	−19.96	−20.07	−20.26	−20.51	−20.76	−21.37	−21.63
2.5	−20.85	−20.23	−20.42	−20.55	−20.77	−21.07	−21.36	−22.05	−22.33
3.0	−21.11	−20.53	−20.75	−20.90	−21.15	−21.48	−21.82	−22.57	−22.89
3.5	−21.23	−20.68	−20.93	−21.10	−21.37	−21.74	−22.11	−22.94	−23.30
4.0	−21.25	−20.75	−21.05	−21.23	−21.51	−21.91	−22.31	−23.18	−23.57
4.5	−21.25	−20.78	−21.10	−21.30	−21.60	−22.02	−22.45	−23.36	−23.77
5.0	−21.34	−20.87	−21.20	−21.41	−21.72	−22.15	−22.59	−23.52	−23.95
5.5	−21.53	−21.04	−21.37	−21.58	−21.89	−22.32	−22.77	−23.71	−24.15
6.0	−21.62	−21.14	−21.48	−21.69	−22.01	−22.45	−22.92	−23.88	−24.33
6.5	−21.78	−21.36	−21.73	−21.95	−22.27	−22.73	−23.19	−24.11	−24.53
7.0	−21.50	−21.06	−21.45	−21.67	−22.00	−22.46	−22.97	−23.99	−24.50
7.5	−21.46	−21.02	−21.42	−21.65	−21.99	−22.47	−22.97	−23.98	−24.50
8.0	−21.41	−20.99	−21.40	−21.64	−21.99	−22.46	−22.95	−23.91	−24.41
8.5	−21.67	−21.28	−21.73	−21.97	−22.33	−22.82	−23.33	−24.30	−24.76
9.0	−21.42	−21.07	−21.56	−21.83	−22.21	−22.73	−23.27	−24.25	−24.72
9.5	−21.36	−21.00	−21.51	−21.78	−22.18	−22.72	−23.27	−24.27	−24.73
10.0	−21.25	−20.91	−21.43	−21.71	−22.11	−22.66	−23.23	−24.25	−24.73
10.5	−21.57	−21.19	−21.68	−21.94	−22.32	−22.83	−23.36	−24.34	−24.81
11.0	−21.49	−21.14	−21.65	−21.92	−22.30	−22.82	−23.36	−24.36	−24.83
11.5	−21.19	−20.89	−21.46	−21.75	−22.15	−22.71	−23.27	−24.28	−24.76
12.0	−21.12	−20.85	−21.43	−21.73	−22.15	−22.72	−23.30	−24.32	−24.79
12.5	−21.25	−20.96	−21.54	−21.83	−22.24	−22.79	−23.34	−24.33	−24.79
13.0	−21.08	−20.84	−21.45	−21.75	−22.17	−22.73	−23.30	−24.29	−24.77
13.5	−20.89	−20.68	−21.32	−21.63	−22.06	−22.64	−23.23	−24.25	−24.74

Table A.5. Apparent integrated SDSS magnitudes of the Salpeter model.

t[Gyr]	Redshift	$m - M$	$m_{\rm Bol}$	m_{V_j}	m_u	m_g	m_r	m_i	m_z
0.5	9.5116	49.953869	39.968	161.915	162.836	162.254	161.664	161.259	52.997
1.0	5.6177	48.640133	33.535	39.367	59.169	56.694	36.545	34.365	32.700
1.5	4.0444	47.801151	30.919	31.566	48.184	32.844	31.073	30.684	30.748
2.0	3.1576	47.159698	29.177	29.381	34.035	29.857	29.311	29.372	29.479
2.5	2.5758	46.626331	27.854	28.294	29.258	28.404	28.318	28.430	28.454
3.0	2.1589	46.160126	26.821	27.528	27.922	27.517	27.579	27.665	27.552
3.5	1.8422	45.738579	26.005	26.979	27.111	26.944	27.052	26.996	26.843
4.0	1.5915	45.347797	25.320	26.548	26.479	26.487	26.562	26.385	26.177
4.5	1.3868	44.978645	24.600	25.928	25.882	25.883	25.870	25.672	25.298
5.0	1.2156	44.624722	24.237	25.664	25.623	25.670	25.548	25.368	24.711
5.5	1.0696	44.281029	23.527	24.984	24.968	25.052	24.871	24.586	23.952
6.0	0.9432	43.943302	23.092	24.549	24.631	24.685	24.422	23.904	23.449
6.5	0.8322	43.607937	22.592	24.174	24.382	24.364	24.034	23.302	22.975
7.0	0.7336	43.271690	22.198	23.744	24.058	23.957	23.527	22.787	22.564
7.5	0.6453	42.931248	21.575	23.130	23.554	23.375	22.755	22.122	21.889
8.0	0.5655	42.583164	21.170	22.682	23.287	22.984	22.194	21.681	21.447
8.5	0.4928	42.223686	20.731	22.159	22.947	22.569	21.636	21.233	20.986
9.0	0.4263	41.848011	20.347	21.657	22.644	22.199	21.176	20.853	20.594
9.5	0.3650	41.450405	19.758	20.903	22.011	21.509	20.525	20.235	20.010
10.0	0.3082	41.023094	19.317	20.355	21.580	20.974	20.071	19.777	19.564
10.5	0.2554	40.554939	18.806	19.785	21.077	20.368	19.548	19.255	19.043
11.0	0.2061	40.029339	18.292	19.237	20.578	19.776	19.023	18.729	18.505
11.5	0.1599	39.418262	17.476	18.362	19.725	18.842	18.174	17.900	17.671
12.0	0.1165	38.670574	16.667	17.526	18.921	17.948	17.337	17.081	16.828
12.5	0.0756	37.670452	15.716	16.566	18.008	16.941	16.356	16.092	15.836
13.0	0.0369	36.051773	14.108	14.932	16.398	15.274	14.713	14.456	14.192
13.5	0.0000	24.999989	3.011	3.807	5.245	4.138	3.596	3.330	3.065

Table A.6. Apparent integrated HST magnitudes of the Salpeter model.

Redshift	m_{U336}	m_{B439}	m_{V555}	m_{V606}	m_{R675}	m_{I814}	m_{J110}	m_{H160}	m_{K222}
9.5116	161.8	162.6	162	161.7	161.2	58.57	39.79	36.96	36.71
5.6177	57.42	59.80	39.05	36.33	34.78	32.76	32.09	31.68	31.27
4.0444	47.64	36.83	31.89	31.16	30.42	30.23	30.11	29.59	28.45
3.1576	39.10	30.20	29.54	29.30	29.06	28.94	28.76	27.76	26.83
2.5758	28.93	28.73	28.30	28.20	28.08	27.96	27.63	26.27	25.53
2.1589	26.85	27.62	27.53	27.46	27.36	27.11	26.57	25.28	24.50
1.8422	26.07	27.07	26.98	26.90	26.78	26.42	25.70	24.48	23.64
1.5915	25.40	26.61	26.52	26.43	26.21	25.80	24.94	23.77	22.90
1.3868	24.66	25.98	25.92	25.78	25.49	24.97	24.15	23.07	22.17
1.2156	24.43	25.76	25.67	25.49	25.18	24.50	23.77	22.75	21.85
1.0696	23.79	25.16	25.02	24.82	24.51	23.72	23.07	22.05	21.14
0.9432	23.42	24.85	24.61	24.38	24.03	23.12	22.58	21.59	20.77
0.8322	23.16	24.57	24.24	23.96	23.46	22.61	22.08	20.98	20.12
0.7336	22.83	24.19	23.81	23.46	22.86	22.16	21.67	20.61	19.80
0.6453	22.34	23.62	23.19	22.76	22.10	21.49	20.98	19.91	19.15
0.5655	22.07	23.24	22.74	22.27	21.59	21.06	20.55	19.49	18.74
0.4928	21.75	22.83	22.24	21.75	21.11	20.61	20.08	19.04	18.28
0.4263	21.50	22.47	21.79	21.30	20.72	20.22	19.67	18.64	17.84
0.3650	20.88	21.82	21.08	20.63	20.09	19.61	19.09	18.11	17.30
0.3082	20.47	21.38	20.55	20.13	19.66	19.17	18.64	17.68	16.84
0.2554	19.99	20.89	19.97	19.58	19.14	18.64	18.11	17.17	16.37
0.2061	19.50	20.32	19.38	19.03	18.60	18.11	17.58	16.64	15.91
0.1599	18.65	19.38	18.49	18.16	17.75	17.28	16.77	15.86	15.20
0.1165	17.85	18.43	17.64	17.33	16.92	16.45	15.94	15.03	14.44
0.0756	16.93	17.37	16.66	16.35	15.94	15.46	14.95	14.04	13.49
0.0369	15.33	15.66	15.01	14.72	14.31	13.81	13.33	12.41	11.93
0.0000	4.23	4.47	3.88	3.60	3.20	2.69	2.22	1.31	0.90

Table A.7. Apparent integrated SDSS magnitudes of the Kroupa model.

t[Gyr]	m_{Bol}	m_{V_j}	m_u	m_g	m_r	m_i	m_z
0.5	39.713	161.914	162.834	162.252	161.663	161.257	52.725
1.0	33.463	39.350	59.066	56.723	36.533	34.342	32.664
1.5	30.902	31.608	48.202	32.899	31.100	30.697	30.752
2.0	29.206	29.453	34.143	29.948	29.375	29.425	29.524
2.5	27.931	28.400	29.396	28.517	28.417	28.521	28.542
3.0	26.905	27.635	28.073	27.635	27.681	27.761	27.638
3.5	26.070	27.051	27.189	27.019	27.122	27.068	26.925
4.0	25.406	26.659	26.604	26.604	26.674	26.499	26.301
4.5	24.805	26.265	26.207	26.214	26.183	25.967	25.581
5.0	24.177	25.705	25.682	25.723	25.567	25.377	24.708
5.5	23.493	25.002	25.018	25.100	24.872	24.582	23.936
6.0	22.906	24.446	24.553	24.602	24.318	23.810	23.343
6.5	22.274	23.846	24.136	24.079	23.700	22.960	22.632
7.0	22.016	23.639	23.986	23.857	23.432	22.697	22.474
7.5	21.584	23.215	23.670	23.440	22.856	22.260	22.037
8.0	21.177	22.754	23.359	23.031	22.279	21.801	21.571
8.5	20.399	21.919	22.669	22.298	21.407	21.015	20.754
9.0	20.074	21.521	22.521	22.055	21.037	20.700	20.409
9.5	19.601	20.937	22.071	21.544	20.555	20.223	19.946
10.0	19.139	20.381	21.640	21.010	20.085	19.736	19.472
10.5	18.376	19.466	20.693	20.040	19.233	18.926	18.702
11.0	17.796	18.847	20.151	19.391	18.635	18.321	18.087
11.5	17.275	18.328	19.749	18.837	18.107	17.771	17.494
12.0	16.448	17.490	18.954	17.946	17.258	16.939	16.625
12.5	15.301	16.269	17.713	16.657	16.034	15.746	15.457
13.0	13.690	14.640	16.146	15.008	14.389	14.101	13.791
13.5	2.656	3.595	5.120	3.968	3.348	3.042	2.708

Table A.8. Apparent integrated HST magnitudes of the Kroupa model.

Redshift	m_{U336}	m_{B439}	m_{V555}	m_{V606}	m_{R675}	m_{I814}	m_{J110}	m_{H160}	m_{K222}
9.5116	161.8	162.6	162	161.7	161.2	58.14	39.58	36.74	36.49
5.6177	57.31	59.76	39.03	36.31	34.76	32.72	32.05	31.63	31.19
4.0444	47.65	36.89	31.93	31.19	30.44	30.24	30.11	29.57	28.39
3.1576	39.21	30.30	29.62	29.37	29.12	28.99	28.80	27.78	26.83
2.5758	29.07	28.85	28.40	28.31	28.17	28.05	27.72	26.34	25.62
2.1589	27.00	27.75	27.65	27.57	27.46	27.21	26.65	25.36	24.59
1.8422	26.15	27.15	27.05	26.97	26.85	26.50	25.79	24.58	23.74
1.5915	25.53	26.73	26.64	26.54	26.32	25.92	25.06	23.89	23.01
1.3868	24.99	26.30	26.25	26.10	25.79	25.25	24.41	23.29	22.31
1.2156	24.49	25.81	25.72	25.52	25.19	24.51	23.75	22.66	21.66
1.0696	23.85	25.22	25.05	24.83	24.51	23.70	23.05	22.00	21.02
0.9432	23.35	24.78	24.51	24.28	23.93	23.02	22.46	21.39	20.44
0.8322	22.91	24.32	23.92	23.63	23.13	22.27	21.74	20.64	19.74
0.7336	22.76	24.10	23.70	23.36	22.77	22.08	21.56	20.42	19.50
0.6453	22.45	23.69	23.27	22.86	22.21	21.64	21.11	19.94	19.05
0.5655	22.14	23.28	22.80	22.35	21.70	21.18	20.65	19.49	18.66
0.4928	21.48	22.55	21.99	21.51	20.89	20.38	19.83	18.66	17.82
0.4263	21.40	22.32	21.65	21.16	20.58	20.04	19.45	18.26	17.38
0.3650	20.97	21.85	21.11	20.66	20.11	19.57	18.95	17.77	16.87
0.3082	20.55	21.42	20.58	20.15	19.65	19.10	18.46	17.30	16.37
0.2554	19.60	20.54	19.65	19.26	18.82	18.30	17.72	16.65	15.79
0.2061	19.07	19.93	19.00	18.64	18.20	17.70	17.10	16.05	15.26
0.1599	18.69	19.39	18.46	18.11	17.65	17.13	16.50	15.44	14.72
0.1165	17.89	18.45	17.61	17.26	16.81	16.27	15.63	14.58	13.91
0.0756	16.63	17.10	16.37	16.04	15.61	15.10	14.49	13.48	12.90
0.0369	15.08	15.40	14.73	14.40	13.97	13.43	12.84	11.83	11.28
0.0000	4.11	4.32	3.68	3.37	2.94	2.36	1.77	0.75	0.26

Appendix B: Mass-to-light ratios

Table B.1. Stellar mass-to-light ratios of the Salpeter model.

t[Gyr]	M/L_{Bol}	M/L_{V_j}	M/L_u	M/L_g	M/L_r	M/L_i	M/L_z	M/L_{J110}	M/L_{H160}	M/L_{K222}
0.5	0.0075	0.1145	0.0137	0.0667	0.1568	0.2202	0.2757	0.4439	0.2919	0.5347
1.0	0.0367	0.1787	0.0435	0.1253	0.2134	0.2503	0.2719	0.4022	0.1886	0.3014
1.5	0.0720	0.2502	0.0759	0.1869	0.2881	0.3218	0.3326	0.4742	0.2012	0.309
2.0	0.1098	0.322	0.1107	0.2511	0.3623	0.391	0.3896	0.5398	0.2143	0.3208
2.5	0.1534	0.4061	0.1533	0.3274	0.4482	0.4689	0.4507	0.6079	0.2261	0.3298
3.0	0.2108	0.5262	0.2136	0.4357	0.5711	0.5807	0.5399	0.7079	0.2463	0.348
3.5	0.2838	0.6727	0.295	0.5715	0.7188	0.7148	0.6483	0.8321	0.2748	0.3793
4.0	0.3602	0.8154	0.3824	0.7088	0.8593	0.839	0.7491	0.9483	0.3035	0.4136
4.5	0.4015	0.8998	0.4271	0.7844	0.9483	0.9292	0.832	1.05	0.3303	0.4407
5.0	0.5645	1.296	0.623	1.137	1.359	1.325	1.179	1.467	0.4342	0.5441
5.5	0.5454	1.301	0.6267	1.151	1.352	1.288	1.111	1.357	0.3998	0.5227
6.0	0.6581	1.482	0.7323	1.313	1.544	1.494	1.323	1.655	0.4988	0.6268
6.5	0.7206	1.628	0.8784	1.496	1.652	1.526	1.285	1.552	0.4505	0.5906
7.0	0.8458	1.871	1.011	1.713	1.913	1.798	1.55	1.892	0.5426	0.6805
7.5	0.7877	1.669	0.9647	1.562	1.68	1.563	1.341	1.65	0.5012	0.6692
8.0	0.8925	1.865	1.109	1.768	1.863	1.718	1.466	1.802	0.5488	0.7315
8.5	0.9728	2.021	1.245	1.934	2.008	1.84	1.559	1.904	0.5707	0.7559
9.0	1.121	2.343	1.489	2.273	2.304	2.082	1.74	2.111	0.6248	0.8199
9.5	1.08	2.25	1.417	2.175	2.221	2.026	1.707	2.085	0.6267	0.8307
10.0	1.219	2.56	1.629	2.488	2.516	2.274	1.901	2.309	0.6847	0.8951
10.5	1.327	2.809	1.828	2.757	2.742	2.457	2.038	2.466	0.7279	0.949
11.0	1.513	3.212	2.14	3.182	3.118	2.766	2.276	2.741	0.7978	1.022
11.5	1.402	2.945	1.98	2.916	2.862	2.561	2.118	2.56	0.7557	0.9879
12.0	1.476	3.093	2.138	3.093	2.989	2.652	2.179	2.625	0.7718	1.012
12.5	1.71	3.583	2.6	3.646	3.425	2.999	2.433	2.912	0.8453	1.093
13.0	1.902	3.953	2.982	4.063	3.761	3.279	2.658	3.177	0.9181	1.173
13.5	2.001	4.166	3.213	4.326	3.938	3.411	2.747	3.282	0.9491	1.218

Table B.2. Stellar mass-to-light ratios of the Kroupa model.

t[Gyr]	M/L_{Bol}	M/L_{V_j}	M/L_u	M/L_g	M/L_r	M/L_i	M/L_z	M/L_{J110}	M/L_{H160}	M/L_{K222}
0.5	0.0056	0.0643	0.0095	0.0397	0.0876	0.1255	0.1586	0.2544	0.1664	0.3011
1.0	0.0288	0.1279	0.0330	0.0905	0.1563	0.1876	0.2012	0.2895	0.13	0.2078
1.5	0.0568	0.1873	0.0586	0.1401	0.2198	0.2487	0.2533	0.3516	0.1428	0.2188
2.0	0.0878	0.2487	0.0877	0.1936	0.2837	0.3079	0.302	0.4078	0.1545	0.2295
2.5	0.1242	0.3261	0.1248	0.2624	0.3635	0.38	0.3595	0.4722	0.1671	0.2406
3.0	0.168	0.4162	0.1706	0.3436	0.4551	0.4618	0.4243	0.5431	0.1808	0.2524
3.5	0.225	0.5502	0.24	0.4649	0.5907	0.5842	0.5211	0.6501	0.2029	0.2727
4.0	0.2985	0.6991	0.3282	0.6044	0.7388	0.7154	0.6259	0.7665	0.2292	0.2996
4.5	0.3742	0.8661	0.4285	0.7648	0.9011	0.855	0.7344	0.8854	0.2556	0.3266
5.0	0.4228	0.9892	0.4967	0.8816	1.022	0.9623	0.8183	0.9774	0.2773	0.3491
5.5	0.4385	1.05	0.5175	0.9357	1.083	1.018	0.8613	1.023	0.2886	0.3614
6.0	0.4868	1.164	0.5874	1.045	1.195	1.115	0.9344	1.101	0.3046	0.3747
6.5	0.5041	1.119	0.6056	1.023	1.137	1.054	0.8777	1.036	0.2966	0.3761
7.0	0.6922	1.66	0.8967	1.524	1.679	1.541	1.269	1.461	0.3804	0.4416
7.5	0.7932	1.903	1.05	1.769	1.906	1.729	1.413	1.633	0.4303	0.4959
8.0	0.9195	2.136	1.214	2.006	2.128	1.923	1.576	1.84	0.5057	0.6008
8.5	0.7509	1.727	1.041	1.653	1.697	1.526	1.234	1.416	0.3869	0.4764
9.0	0.9319	2.159	1.4	2.129	2.082	1.82	1.438	1.628	0.4367	0.5333
9.5	1.016	2.417	1.593	2.413	2.31	1.992	1.551	1.74	0.4606	0.5646
10.0	1.139	2.753	1.859	2.773	2.614	2.233	1.722	1.913	0.4981	0.6033
10.5	0.9963	2.333	1.493	2.297	2.251	1.991	1.582	1.791	0.4844	0.5899
11.0	1.078	2.516	1.676	2.506	2.409	2.118	1.67	1.88	0.5029	0.6079
11.5	1.321	3.107	2.266	3.206	2.913	2.484	1.916	2.136	0.5639	0.6761
12.0	1.377	3.295	2.492	3.453	3.058	2.574	1.958	2.159	0.5642	0.6833
12.5	1.342	3.098	2.305	3.217	2.896	2.486	1.924	2.151	0.5789	0.7083
13.0	1.5	3.47	2.749	3.667	3.212	2.724	2.091	2.323	0.6177	0.744
13.5	1.683	3.997	3.34	4.315	3.656	3.052	2.307	2.534	0.6603	0.7859

Table B.3. Stellar mass-to-light ratios of the absorptionless Salpeter model.

t[Gyr]	M/L_{Bol}	M/L_{V_j}	M/L_u	M/L_g	M/L_r	M/L_i	M/L_z	M/L_{J110}	M/L_{H160}	M/L_{K222}
0.5	0.0075	0.1145	0.0137	0.0667	0.1568	0.2202	0.2757	0.4439	0.2919	0.5347
1.0	0.0339	0.1725	0.0413	0.1201	0.207	0.2443	0.2672	0.3966	0.1874	0.3006
1.5	0.0594	0.2257	0.0658	0.1655	0.2633	0.2998	0.3153	0.4541	0.1975	0.3062
2.0	0.0810	0.2681	0.0862	0.2024	0.3081	0.3434	0.353	0.4991	0.2071	0.3158
2.5	0.0995	0.3038	0.1041	0.2343	0.346	0.3801	0.3839	0.5349	0.2133	0.3208
3.0	0.1213	0.3461	0.125	0.2714	0.3908	0.4238	0.4214	0.5796	0.2238	0.3323
3.5	0.1557	0.4113	0.159	0.3292	0.4586	0.4896	0.4788	0.6501	0.2433	0.3573
4.0	0.1963	0.4918	0.2018	0.4023	0.5407	0.5667	0.5462	0.7314	0.2653	0.386
4.5	0.2237	0.5563	0.2321	0.4606	0.6066	0.6277	0.595	0.7858	0.277	0.3986
5.0	0.2941	0.68	0.3119	0.5777	0.7306	0.7435	0.6971	0.9122	0.3157	0.4513
5.5	0.3115	0.7432	0.3372	0.6337	0.7949	0.8044	0.7494	0.977	0.335	0.4772
6.0	0.3521	0.8217	0.3826	0.7065	0.874	0.8797	0.8142	1.059	0.3607	0.5123
6.5	0.4124	0.9291	0.4521	0.8107	0.9792	0.9738	0.8914	1.15	0.3866	0.5461
7.0	0.4761	1.05	0.5317	0.9308	1.097	1.078	0.9774	1.253	0.4154	0.5846
7.5	0.5405	1.18	0.6177	1.06	1.222	1.189	1.069	1.361	0.4467	0.6257
8.0	0.5891	1.288	0.682	1.164	1.327	1.284	1.146	1.454	0.4736	0.6604
8.5	0.6626	1.428	0.7857	1.307	1.46	1.4	1.239	1.566	0.5059	0.7035
9.0	0.7341	1.564	0.885	1.446	1.59	1.511	1.33	1.672	0.5367	0.7429
9.5	0.781	1.682	0.9564	1.563	1.702	1.612	1.409	1.768	0.5642	0.7788
10.0	0.8262	1.789	1.021	1.668	1.808	1.704	1.483	1.855	0.5898	0.8119
10.5	0.8997	1.929	1.134	1.815	1.938	1.815	1.571	1.961	0.6201	0.8521
11.0	0.9628	2.053	1.226	1.942	2.053	1.914	1.649	2.051	0.6455	0.8837
11.5	1.045	2.208	1.357	2.11	2.195	2.032	1.739	2.157	0.676	0.9228
12.0	1.121	2.368	1.483	2.28	2.339	2.153	1.831	2.263	0.7046	0.9592
12.5	1.217	2.553	1.65	2.488	2.509	2.292	1.935	2.382	0.7376	0.9996
13.0	1.374	2.803	1.938	2.78	2.727	2.466	2.065	2.531	0.7785	1.051
13.5	1.438	2.996	2.065	2.987	2.901	2.607	2.17	2.653	0.8115	1.094

Table B.4. Stellar mass-to-light ratios of the absorptionless Kroupa model.

t[Gyr]	M/L_{Bol}	M/L_{V_j}	M/L_u	M/L_g	M/L_r	M/L_i	M/L_z	M/L_{J110}	M/L_{H160}	M/L_{K222}
0.5	0.0056	0.0643	0.0095	0.0397	0.0876	0.1255	0.1586	0.2544	0.1664	0.3011
1.0	0.0264	0.1229	0.0311	0.0863	0.151	0.1825	0.1972	0.285	0.1291	0.2071
1.5	0.0461	0.167	0.0500	0.1225	0.1988	0.2295	0.2386	0.3352	0.1398	0.2166
2.0	0.0638	0.2034	0.0668	0.1532	0.2373	0.2665	0.2707	0.374	0.1485	0.2253
2.5	0.0782	0.2356	0.0814	0.1807	0.271	0.2985	0.2982	0.4068	0.1558	0.2326
3.0	0.0934	0.2677	0.0965	0.2088	0.3043	0.33	0.3252	0.4382	0.163	0.2397
3.5	0.114	0.3103	0.1176	0.246	0.3478	0.371	0.3605	0.4801	0.1737	0.252
4.0	0.1438	0.3682	0.1484	0.2979	0.4071	0.4271	0.4086	0.5377	0.1892	0.271
4.5	0.173	0.4305	0.181	0.3545	0.4699	0.4852	0.4575	0.5953	0.2047	0.2897
5.0	0.1976	0.4867	0.209	0.4052	0.5269	0.5396	0.5022	0.647	0.2186	0.306
5.5	0.2017	0.5156	0.2173	0.4293	0.5576	0.5696	0.5272	0.6747	0.2259	0.3136
6.0	0.2142	0.5447	0.2296	0.4539	0.5879	0.5988	0.5492	0.6978	0.2308	0.3178
6.5	0.2504	0.6044	0.2683	0.5097	0.6471	0.6531	0.5918	0.7429	0.2415	0.3279
7.0	0.3069	0.7175	0.3422	0.6221	0.7548	0.7486	0.6715	0.8353	0.2668	0.3589
7.5	0.3425	0.802	0.3903	0.7037	0.8368	0.823	0.7315	0.9041	0.2859	0.3832
8.0	0.3777	0.8829	0.4368	0.7804	0.9152	0.8944	0.7891	0.9699	0.3045	0.4062
8.5	0.4192	0.9718	0.4934	0.8677	1.001	0.97	0.848	1.035	0.3215	0.4269
9.0	0.4714	1.082	0.5693	0.9794	1.104	1.06	0.9183	1.113	0.3424	0.4527
9.5	0.5102	1.177	0.6271	1.074	1.195	1.14	0.9802	1.182	0.3605	0.4739
10.0	0.5625	1.286	0.7056	1.186	1.297	1.23	1.05	1.258	0.3807	0.4986
10.5	0.6087	1.393	0.7769	1.294	1.397	1.316	1.115	1.329	0.3992	0.5204
11.0	0.6648	1.51	0.8659	1.416	1.505	1.409	1.185	1.404	0.419	0.5438
11.5	0.7284	1.653	0.979	1.572	1.635	1.518	1.268	1.494	0.4426	0.5717
12.0	0.7717	1.765	1.05	1.684	1.739	1.608	1.335	1.565	0.4607	0.5935
12.5	0.8399	1.908	1.172	1.839	1.868	1.716	1.415	1.65	0.4824	0.6186
13.0	0.9094	2.064	1.307	2.012	2.006	1.831	1.498	1.739	0.5053	0.6456
13.5	0.9867	2.238	1.465	2.207	2.161	1.956	1.59	1.836	0.5304	0.6751

Appendix C: Correction tables

Table C.1. Absorption corrections $m_{X,includingabs.} - m_{X,abs.less}$ for the Kroupa model in the SDSS system.

Redshift	BOL	V_j	u	g	r	i	z
9.5116	0	0	0	0	0	0	0
5.6177	0.081	0.152	0.258	0.151	0.151	0.124	0.105
4.0444	0.210	0.339	0.498	0.378	0.294	0.259	0.254
3.1576	0.331	0.447	0.631	0.506	0.420	0.412	0.458
2.5758	0.488	0.627	0.827	0.669	0.620	0.677	0.607
2.1589	0.625	0.820	0.974	0.840	0.848	0.849	0.711
1.8422	0.727	0.992	1.037	0.966	1.045	0.912	0.824
1.5915	0.783	1.157	1.123	1.094	1.117	0.959	0.876
1.3868	0.828	1.247	1.187	1.224	1.121	0.998	0.911
1.2156	0.820	1.163	1.166	1.233	1.060	0.965	0.893
1.0696	0.837	1.105	1.179	1.234	1.027	0.934	0.878
0.9432	0.886	1.147	1.278	1.291	1.081	0.980	0.917
0.8322	0.757	0.991	1.241	1.147	0.918	0.818	0.736
0.7336	0.880	1.094	1.339	1.183	1.044	0.999	0.938
0.6453	0.908	1.101	1.402	1.178	1.052	1.016	0.941
0.5655	0.962	1.115	1.446	1.195	1.070	1.022	0.945
0.4928	0.631	0.794	1.089	0.873	0.753	0.668	0.585
0.4263	0.738	0.932	1.272	1.027	0.886	0.776	0.681
0.3650	0.746	0.952	1.243	1.032	0.905	0.781	0.683
0.3082	0.765	0.977	1.238	1.045	0.924	0.801	0.704
0.2554	0.534	0.649	0.801	0.692	0.607	0.530	0.469
0.2061	0.524	0.634	0.801	0.684	0.584	0.509	0.445
0.1599	0.645	0.773	1.008	0.845	0.702	0.606	0.520
0.1165	0.629	0.754	1.020	0.842	0.673	0.570	0.474
0.0756	0.508	0.564	0.774	0.640	0.506	0.431	0.360
0.0369	0.543	0.584	0.831	0.672	0.526	0.447	0.374
0.0000	0.580	0.630	0.895	0.728	0.571	0.483	0.404

Table C.2. Absorption corrections $m_{X,includingabs.} - m_{X,abs.less}$ for the Kroupa model in the HST system.

Redshift	U336	B439	V555	V606	R675	I814	J110	H160	K222
9.5116	0	0	0	0	0	0	0	0	0
5.6177	0.267	0.199	0.151	0.143	0.139	0.107	0.100	0.100	0.065
4.0444	0.546	0.422	0.340	0.307	0.276	0.255	0.261	0.191	0.154
3.1576	0.627	0.553	0.459	0.435	0.413	0.436	0.396	0.283	0.222
2.5758	0.869	0.705	0.641	0.629	0.634	0.649	0.536	0.419	0.317
2.1589	1.024	0.862	0.824	0.841	0.887	0.770	0.641	0.516	0.391
1.8422	1.069	0.967	0.986	1.004	1.004	0.861	0.757	0.617	0.472
1.5915	1.157	1.079	1.125	1.114	1.028	0.912	0.805	0.651	0.484
1.3868	1.215	1.177	1.230	1.177	1.053	0.944	0.842	0.674	0.495
1.2156	1.169	1.201	1.199	1.119	1.012	0.918	0.824	0.651	0.473
1.0696	1.180	1.266	1.157	1.071	0.985	0.897	0.802	0.619	0.442
0.9432	1.270	1.375	1.188	1.115	1.032	0.942	0.830	0.628	0.453
0.8322	1.204	1.258	1.029	0.950	0.863	0.771	0.646	0.446	0.305
0.7336	1.289	1.249	1.112	1.063	1.015	0.966	0.868	0.683	0.506
0.6453	1.373	1.230	1.117	1.072	1.034	0.975	0.870	0.685	0.527
0.5655	1.469	1.241	1.133	1.088	1.052	0.977	0.870	0.712	0.582
0.4928	1.142	0.918	0.811	0.763	0.717	0.619	0.508	0.339	0.219
0.4263	1.367	1.081	0.951	0.898	0.840	0.720	0.584	0.391	0.268
0.3650	1.329	1.087	0.965	0.915	0.850	0.724	0.577	0.379	0.257
0.3082	1.309	1.099	0.987	0.937	0.866	0.745	0.593	0.393	0.272
0.2554	0.839	0.722	0.656	0.620	0.568	0.495	0.400	0.271	0.183
0.2061	0.836	0.716	0.643	0.602	0.546	0.473	0.377	0.251	0.161
0.1599	1.057	0.887	0.788	0.730	0.654	0.556	0.442	0.306	0.214
0.1165	1.072	0.891	0.774	0.706	0.624	0.514	0.392	0.249	0.171
0.0756	0.814	0.683	0.584	0.532	0.470	0.389	0.308	0.211	0.157
0.0369	0.880	0.725	0.606	0.552	0.489	0.404	0.325	0.225	0.160
0.0000	0.945	0.785	0.655	0.596	0.531	0.436	0.350	0.238	0.165

Table C.3. Inclination corrections $m_{X,\text{diagonal}} - m_{X,\text{faceon}}$ for the Kroupa model in the SDSS system.

Redshift	BOL	V_j	u	g	r	i	z
9.5116	0	0	0	0	0	0	0
5.6177	0.037	0.065	0.079	0.049	0.064	0.055	0.047
4.0444	0.071	0.110	0.121	0.121	0.098	0.088	0.086
3.1576	0.119	0.160	0.211	0.174	0.152	0.151	0.163
2.5758	0.170	0.219	0.257	0.227	0.218	0.233	0.217
2.1589	0.243	0.329	0.378	0.336	0.337	0.335	0.290
1.8422	0.275	0.378	0.377	0.365	0.396	0.358	0.334
1.5915	0.332	0.501	0.485	0.476	0.485	0.422	0.388
1.3868	0.365	0.567	0.539	0.557	0.509	0.453	0.412
1.2156	0.378	0.557	0.553	0.591	0.506	0.460	0.424
1.0696	0.397	0.543	0.578	0.609	0.503	0.454	0.425
0.9432	0.436	0.597	0.657	0.667	0.563	0.508	0.475
0.8322	0.218	0.347	0.475	0.424	0.311	0.264	0.226
0.7336	0.260	0.390	0.456	0.415	0.375	0.361	0.338
0.6453	0.304	0.427	0.551	0.464	0.403	0.377	0.341
0.5655	0.360	0.455	0.594	0.493	0.432	0.402	0.363
0.4928	0.036	0.141	0.239	0.174	0.118	0.064	0.019
0.4263	0.133	0.275	0.445	0.326	0.239	0.165	0.102
0.3650	0.157	0.320	0.504	0.376	0.277	0.188	0.118
0.3082	0.176	0.330	0.502	0.382	0.285	0.197	0.129
0.2554	−0.049	0.006	0.082	0.037	−0.023	−0.069	−0.100
0.2061	−0.095	−0.056	0.024	−0.022	−0.082	−0.124	−0.154
0.1599	0.058	0.119	0.302	0.183	0.065	−0.008	−0.066
0.1165	0.007	0.092	0.295	0.166	0.030	−0.049	−0.120
0.0756	−0.098	−0.116	0.063	−0.055	−0.160	−0.210	−0.252
0.0369	−0.083	−0.113	0.075	−0.049	−0.157	−0.208	−0.254
0.0000	−0.008	−0.024	0.179	0.049	−0.069	−0.129	−0.183

Table C.4. Inclination corrections $m_{X,\text{diagonal}} - m_{X,\text{faceon}}$ for the Kroupa model in the HST system.

Redshift	$U336$	$B439$	$V555$	$V606$	$R675$	$I814$	$J110$	$H160$	$K222$
9.5116	0	0	0	0	0	0	0	0	0
5.6177	0.081	0.062	0.065	0.061	0.060	0.048	0.045	0.045	0.030
4.0444	0.128	0.137	0.110	0.101	0.093	0.087	0.088	0.067	0.054
3.1576	0.206	0.184	0.163	0.157	0.151	0.158	0.145	0.111	0.090
2.5758	0.267	0.234	0.222	0.220	0.222	0.226	0.198	0.167	0.134
2.1589	0.392	0.345	0.330	0.334	0.348	0.310	0.262	0.213	0.170
1.8422	0.379	0.363	0.374	0.382	0.384	0.344	0.313	0.269	0.218
1.5915	0.498	0.468	0.489	0.484	0.450	0.403	0.357	0.298	0.235
1.3868	0.554	0.536	0.559	0.534	0.479	0.428	0.383	0.317	0.250
1.2156	0.553	0.574	0.574	0.535	0.484	0.437	0.393	0.318	0.245
1.0696	0.576	0.626	0.569	0.525	0.481	0.435	0.390	0.310	0.236
0.9432	0.652	0.710	0.616	0.579	0.537	0.488	0.432	0.333	0.243
0.8322	0.457	0.481	0.366	0.326	0.285	0.242	0.182	0.079	−0.002
0.7336	0.443	0.433	0.396	0.381	0.366	0.349	0.309	0.216	0.097
0.6453	0.542	0.488	0.436	0.412	0.391	0.357	0.303	0.198	0.113
0.5655	0.603	0.516	0.463	0.440	0.420	0.379	0.324	0.238	0.190
0.4928	0.248	0.195	0.148	0.121	0.090	0.038	−0.018	−0.114	−0.143
0.4263	0.482	0.357	0.284	0.247	0.205	0.128	0.042	−0.081	−0.099
0.3650	0.546	0.411	0.328	0.288	0.237	0.147	0.042	−0.106	−0.136
0.3082	0.539	0.417	0.337	0.299	0.245	0.158	0.049	−0.083	−0.085
0.2554	0.095	0.049	0.012	−0.012	−0.045	−0.088	−0.143	−0.197	−0.154
0.2061	0.037	−0.006	−0.048	−0.072	−0.103	−0.141	−0.194	−0.225	−0.162
0.1599	0.336	0.222	0.135	0.086	0.027	−0.042	−0.117	−0.148	−0.083
0.1165	0.331	0.210	0.110	0.055	−0.010	−0.091	−0.188	−0.254	−0.189
0.0756	0.093	−0.011	−0.100	−0.140	−0.185	−0.234	−0.284	−0.272	−0.169
0.0369	0.108	−0.007	−0.099	−0.138	−0.182	−0.235	−0.276	−0.231	−0.126
0.0000	0.212	0.093	−0.006	−0.049	−0.096	−0.161	−0.203	−0.161	−0.079

Table C.5. Inclination corrections $m_{X,\text{edgeon}} - m_{X,\text{faceon}}$ for the Kroupa model in the SDSS system.

Redshift	BOL	V_j	u	g	r	i	z
9.5116	0	0	0	0	0	0	0
5.6177	0.067	0.121	0.145	0.072	0.119	0.1	0.086
4.0444	0.150	0.228	0.203	0.248	0.207	0.189	0.185
3.1576	0.259	0.34	0.419	0.359	0.328	0.326	0.345
2.5758	0.342	0.426	0.478	0.438	0.426	0.447	0.425
2.1589	0.482	0.613	0.637	0.614	0.624	0.625	0.584
1.8422	0.576	0.746	0.746	0.729	0.767	0.723	0.693
1.5915	0.700	0.943	0.918	0.914	0.929	0.870	0.831
1.3868	0.791	1.098	1.063	1.088	1.034	0.969	0.911
1.2156	0.869	1.170	1.172	1.212	1.108	1.040	0.974
1.0696	0.930	1.165	1.185	1.226	1.131	1.078	1.049
0.9432	1.034	1.327	1.374	1.393	1.293	1.220	1.188
0.8322	1.004	1.318	1.382	1.362	1.290	1.236	1.207
0.7336	0.856	1.189	1.286	1.228	1.156	1.120	1.086
0.6453	0.894	1.226	1.385	1.282	1.179	1.141	1.095
0.5655	0.916	1.261	1.440	1.322	1.217	1.178	1.129
0.4928	0.900	1.252	1.375	1.296	1.229	1.197	1.150
0.4263	0.900	1.279	1.452	1.340	1.254	1.200	1.145
0.3650	0.943	1.360	1.603	1.438	1.325	1.249	1.180
0.3082	0.861	1.311	1.460	1.353	1.282	1.208	1.130
0.2554	0.902	1.338	1.506	1.381	1.298	1.216	1.129
0.2061	0.837	1.318	1.515	1.370	1.264	1.172	1.065
0.1599	0.757	1.293	1.490	1.352	1.224	1.107	0.960
0.1165	0.726	1.297	1.520	1.375	1.213	1.073	0.892
0.0756	0.687	1.229	1.482	1.329	1.136	0.975	0.772
0.0369	0.583	1.127	1.403	1.247	1.025	0.840	0.613
0.0000	0.501	0.957	1.294	1.107	0.848	0.649	0.432

Table C.6. Inclination corrections $m_{X,\text{diagonal}} - m_{X,\text{edgeon}}$ for the Kroupa model in the HST system.

Redshift	$U336$	$B439$	$V555$	$V606$	$R675$	$I814$	$J110$	$H160$	$K222$
9.5116	0	0	0	0	0	0	0	0	0
5.6177	0.150	0.105	0.121	0.114	0.111	0.088	0.083	0.083	0.055
4.0444	0.217	0.289	0.229	0.213	0.198	0.186	0.187	0.145	0.119
3.1576	0.407	0.372	0.344	0.335	0.326	0.336	0.317	0.257	0.214
2.5758	0.493	0.447	0.431	0.428	0.432	0.438	0.400	0.356	0.303
2.1589	0.645	0.622	0.611	0.618	0.636	0.602	0.551	0.492	0.426
1.8422	0.745	0.724	0.741	0.751	0.752	0.705	0.661	0.601	0.525
1.5915	0.930	0.903	0.930	0.927	0.896	0.849	0.791	0.716	0.619
1.3868	1.084	1.065	1.089	1.062	1.000	0.934	0.873	0.788	0.682
1.2156	1.172	1.195	1.189	1.141	1.076	0.996	0.935	0.839	0.731
1.0696	1.175	1.242	1.189	1.150	1.112	1.058	1.015	0.917	0.796
0.9432	1.365	1.432	1.344	1.308	1.262	1.200	1.141	1.018	0.855
0.8322	1.366	1.394	1.328	1.298	1.258	1.219	1.157	1.015	0.815
0.7336	1.269	1.255	1.197	1.166	1.131	1.102	1.039	0.875	0.611
0.6453	1.376	1.314	1.238	1.196	1.156	1.116	1.042	0.858	0.587
0.5655	1.449	1.353	1.274	1.233	1.199	1.150	1.065	0.863	0.567
0.4928	1.394	1.315	1.262	1.239	1.220	1.170	1.078	0.848	0.538
0.4263	1.484	1.371	1.292	1.262	1.233	1.168	1.057	0.796	0.485
0.3650	1.647	1.487	1.376	1.335	1.292	1.210	1.070	0.755	0.413
0.3082	1.490	1.389	1.317	1.289	1.249	1.164	0.992	0.637	0.331
0.2554	1.541	1.421	1.345	1.310	1.259	1.167	0.990	0.649	0.361
0.2061	1.558	1.410	1.326	1.283	1.220	1.111	0.896	0.526	0.274
0.1599	1.528	1.387	1.304	1.249	1.172	1.022	0.747	0.359	0.165
0.1165	1.561	1.412	1.314	1.244	1.152	0.967	0.658	0.252	0.080
0.0756	1.524	1.375	1.253	1.172	1.066	0.856	0.552	0.201	0.080
0.0369	1.448	1.302	1.157	1.063	0.946	0.705	0.400	0.098	0.022
0.0000	1.343	1.184	0.995	0.889	0.762	0.518	0.265	0.050	0.013

Appendix D: Other quantities

Table D.1. Petrosion radii [kpc] for the Kroupa model.

t[Gyr]	petroR90$_{\text{BOL}}$	petroR90$_{Vj}$	petroR90$_u$	petroR90$_g$	petroR90$_r$	petroR90$_i$	petroR90$_z$
0.5	16.69	16.72	16.71	16.72	16.73	16.62	15.56
1.0	3.499	3.348	3.435	3.389	3.312	3.256	3.217
1.5	4.467	4.353	4.451	4.410	4.306	4.233	4.158
2.0	5.704	5.374	5.618	5.474	5.298	5.195	5.104
2.5	6.312	6.184	6.339	6.270	6.118	6.011	5.896
3.0	6.778	6.661	6.821	6.759	6.582	6.454	6.323
3.5	7.465	7.150	7.468	7.299	7.040	6.881	6.720
4.0	7.504	7.424	7.654	7.553	7.326	7.160	6.969
4.5	7.596	7.577	7.772	7.705	7.473	7.301	7.102
5.0	7.860	7.767	8.076	7.938	7.646	7.472	7.246
5.5	7.946	7.902	8.212	8.066	7.781	7.616	7.408
6.0	8.282	8.234	8.459	8.369	8.132	7.980	7.805
6.5	8.611	8.666	8.862	8.797	8.561	8.406	8.197
7.0	8.729	8.885	9.001	8.999	8.785	8.637	8.447
7.5	8.992	9.094	9.261	9.222	8.989	8.821	8.620
8.0	8.907	9.092	9.226	9.211	8.992	8.846	8.647
8.5	9.007	9.096	9.387	9.237	8.986	8.797	8.598
9.0	8.993	9.163	9.360	9.284	9.067	8.916	8.710
9.5	8.830	9.052	9.176	9.164	8.966	8.843	8.677
10.0	8.893	9.095	9.310	9.218	9.002	8.856	8.671
10.5	8.805	9.048	9.283	9.181	8.950	8.809	8.641
11.0	8.778	9.029	9.283	9.157	8.937	8.804	8.641
11.5	8.596	8.903	9.081	9.014	8.820	8.702	8.541
12.0	8.395	8.740	8.827	8.833	8.677	8.582	8.444
12.5	8.445	8.756	8.928	8.858	8.680	8.571	8.419
13.0	8.304	8.671	8.901	8.776	8.601	8.500	8.359
13.5	8.133	8.477	8.717	8.586	8.407	8.310	8.174

Table D.2. Petrosion radii [arcsec] for the Kroupa model.

$redshift$	petroR90$_{\text{BOL}}$	petroR90$_{Vj}$	petroR90$_u$	petroR90$_g$	petroR90$_r$	petroR90$_i$	petroR90$_z$
9.5116	3.886	0	0	0	0	0	3.879
5.6177	0.585	0.610	0.673	1.038	0.615	0.604	0.596
4.0444	0.643	0.665	0.865	0.660	0.655	0.654	0.650
3.1576	0.748	0.794	0.808	0.808	0.790	0.778	0.785
2.5758	0.785	0.809	0.817	0.809	0.807	0.816	0.807
2.1589	0.816	0.836	0.849	0.838	0.839	0.840	0.828
1.8422	0.883	0.925	0.941	0.929	0.928	0.909	0.892
1.5915	0.884	0.931	0.930	0.928	0.927	0.911	0.903
1.3868	0.900	0.939	0.940	0.938	0.932	0.923	0.924
1.2156	0.945	0.992	1.008	1.000	0.984	0.972	0.970
1.0696	0.977	1.028	1.041	1.039	1.018	1.011	1.003
0.9432	1.049	1.079	1.090	1.087	1.074	1.073	1.062
0.8322	1.131	1.168	1.184	1.178	1.164	1.168	1.152
0.7336	1.199	1.235	1.247	1.238	1.237	1.243	1.227
0.6453	1.301	1.340	1.365	1.344	1.346	1.338	1.318
0.5655	1.370	1.419	1.432	1.417	1.429	1.415	1.393
0.4928	1.486	1.549	1.587	1.559	1.545	1.515	1.488
0.4263	1.610	1.680	1.699	1.678	1.675	1.648	1.623
0.3650	1.739	1.818	1.804	1.808	1.810	1.783	1.761
0.3082	1.959	2.050	2.066	2.055	2.030	1.996	1.968
0.2554	2.216	2.326	2.349	2.339	2.301	2.259	2.229
0.2061	2.598	2.718	2.761	2.744	2.689	2.644	2.609
0.1599	3.118	3.267	3.295	3.296	3.237	3.191	3.148
0.1165	3.981	4.176	4.168	4.207	4.142	4.100	4.045
0.0756	5.891	6.141	6.227	6.203	6.084	6.011	5.918
0.0369	11.34	11.88	12.16	12.03	11.77	11.65	11.47
0.0000	1678	1748	1798	1771	1734	1714	1686

Table D.3. Concentration parameters for the Kroupa model.

Redshift	C_{BOL}	C_{Vj}	C_u	C_g	C_r	C_i	C_z
9.5116	–	–	–	–	–	–	–
5.6177	–	–	–	–	–	–	–
4.0444	–	–	–	–	–	–	–
3.1576	–	–	–	–	–	–	–
2.5758	–	–	–	–	–	–	–
2.1589	–	–	–	–	–	–	–
1.8422	–	–	–	–	–	–	–
1.5915	0.234	0.298	0.337	0.311	0.292	0.264	0.237
1.3868	0.135	0.135	0.135	0.135	0.135	0.135	0.134
1.2156	0.229	0.228	0.221	0.230	0.226	0.224	0.220
1.0696	0.290	0.270	0.265	0.277	0.268	0.264	0.265
0.9432	0.378	0.363	0.360	0.370	0.361	0.352	0.353
0.8322	0.398	0.383	0.382	0.384	0.383	0.378	0.379
0.7336	0.297	0.264	0.243	0.255	0.266	0.267	0.274
0.6453	0.284	0.240	0.232	0.236	0.238	0.244	0.250
0.5655	0.311	0.269	0.261	0.268	0.264	0.270	0.278
0.4928	0.319	0.275	0.258	0.274	0.274	0.283	0.291
0.4263	0.324	0.271	0.259	0.271	0.273	0.282	0.291
0.3650	0.353	0.303	0.322	0.313	0.303	0.306	0.311
0.3082	0.371	0.314	0.329	0.320	0.315	0.319	0.323
0.2554	0.387	0.333	0.338	0.334	0.334	0.339	0.344
0.2061	0.410	0.343	0.362	0.346	0.343	0.347	0.352
0.1599	0.441	0.373	0.399	0.378	0.373	0.375	0.382
0.1165	0.456	0.397	0.434	0.405	0.394	0.393	0.401
0.0756	0.492	0.417	0.463	0.425	0.415	0.416	0.427
0.0369	0.517	0.438	0.470	0.443	0.438	0.441	0.455
0.0000	0.556	0.479	0.512	0.484	0.478	0.481	0.497